Article

Cell

Auto-regulation of Secretory Flux by Sensing and Responding to the Folded Cargo Protein Load in the Endoplasmic Reticulum

Graphical Abstract

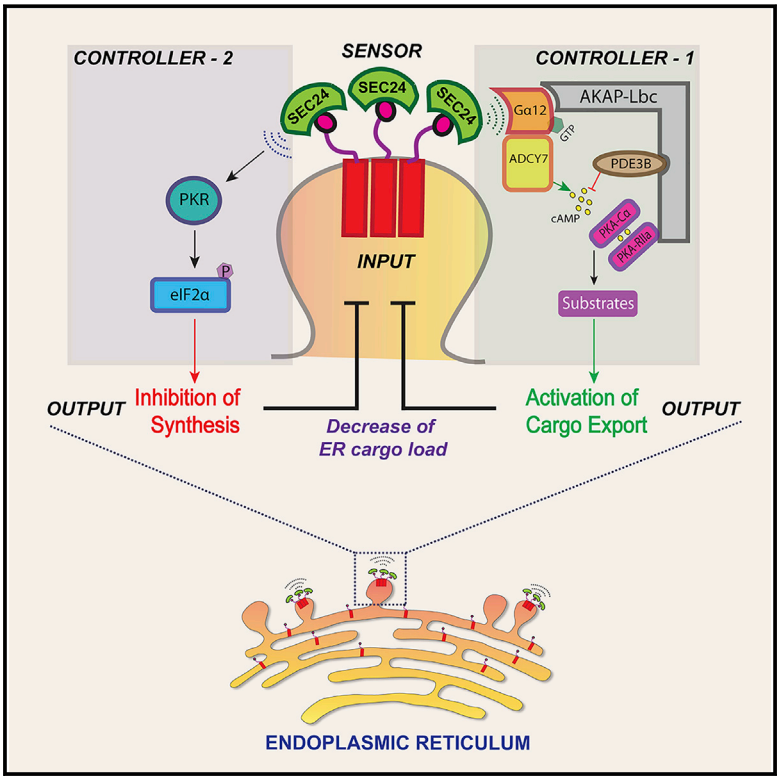

Highlights

- ER exit sites are endowed with an auto-regulatory signaling complex called AREX
- The COPII subunit Sec24 senses folded cargo and activates the AREX signaling network
- AREX responds to folded cargo fluxes by regulating cargo export and protein synthesis
- AREX maintains potentially harmful folded cargo in the ER at steady low levels

Authors

Advait Subramanian, Anita Capalbo, Namrata Ravi Iyengar, ..., Francesca Fanelli, Michele Sallese, Alberto Luini

Correspondence

a.subramanian@ibp.cnr.it (A.S.), a.luini@ibp.cnr.it (A.L.)

In Brief

By sensing the load of folded ER lumenal proteins, the COPII subunit Sec24 directs a signaling cascade that allows secretory pathway flux to respond to the abundance of cargo.

Subramanian et al., 2019, Cell *176*, 1461–1476
March 7, 2019
https://doi.org/10.1016/j.cell.2019.01.035

CellPress

Cell

Auto-regulation of Secretory Flux by Sensing and Responding to the Folded Cargo Protein Load in the Endoplasmic Reticulum

Advait Subramanian,[1,10,11,*] Anita Capalbo,[1,11] Namrata Ravi Iyengar,[1] Riccardo Rizzo,[1] Antonella di Campli,[1,2] Rosaria Di Martino,[1] Matteo Lo Monte,[1] Andrea R. Beccari,[1,3] Amol Yerudkar,[4] Carmen del Vecchio,[4] Luigi Glielmo,[4] Gabriele Turacchio,[1] Marinella Pirozzi,[1] Sang Geon Kim,[5] Petra Henklein,[6] Jorge Cancino,[7] Seetharaman Parashuraman,[1] Dario Diviani,[8] Francesca Fanelli,[9] Michele Sallese,[2] and Alberto Luini[1,12,*]

[1]Institute of Protein Biochemistry (IBP), Italian National Research Council (CNR), Napoli, Italy
[2]Department of Medical, Oral and Biotechnological Sciences and CeSI-MeT, Center for Research on Ageing and Translational Medicine, "G. d'Annunzio" University of Chieti-Pescara, Chieti, Italy
[3]Dompé Farmaceutici SpA, Milan, Italy
[4]Department of Engineering, Universitá degli Studi del Sannio, Benevento, Italy
[5]College of Pharmacy and Research Institute of Pharmaceutical Sciences, Seoul National University, Seoul, South Korea
[6]Institut fur Biochemie, Charite Universitätsmedizin, Berlin, Germany
[7]Centro de Biología Celular y Biomedicina (CEBICEM), Facultad de Medicina y Ciencia, Universidad San Sebastián, Lota 2465, Santiago 7510157, Chile
[8]Université de Lausanne, Département de Pharmacologie et Toxicologie, Rue du Bugnon 27, 1011 Lausanne, Switzerland
[9]Department of Life Sciences, University of Modena and Reggio Emilia, Modena, Italy
[10]Present address: George William Hooper Foundation, Department of Microbiology and Immunology, and Department of Biochemistry and Biophysics, University of California, San Francisco, San Francisco, CA, USA
[11]These authors contributed equally
[12]Lead Contact
*Correspondence: a.subramanian@ibp.cnr.it (A.S.), a.luini@ibp.cnr.it (A.L.)
https://doi.org/10.1016/j.cell.2019.01.035

SUMMARY

Maintaining the optimal performance of cell processes and organelles is the task of auto-regulatory systems. Here we describe an auto-regulatory device that helps to maintain homeostasis of the endoplasmic reticulum (ER) by adjusting the secretory flux to the cargo load. The cargo-recruiting subunit of the coatomer protein II (COPII) coat, Sec24, doubles as a sensor of folded cargo and, upon cargo binding, acts as a guanine nucleotide exchange factor to activate the signaling protein Gα12 at the ER exit sites (ERESs). This step, in turn, activates a complex signaling network that activates and coordinates the ER export machinery and attenuates proteins synthesis, thus preventing large fluctuations of folded and potentially active cargo that could be harmful to the cell or the organism. We call this mechanism AREX (autoregulation of ER export) and expect that its identification will aid our understanding of human physiology and diseases that develop from secretory dysfunction.

INTRODUCTION

An essential property of the secretory pathway is to preserve its compositional and morphological homeostasis and to perform optimally despite the physiological and pathological perturbations to which it is exposed. Therefore, it must maintain tight coordination between the transport and processing activities of its main stations—the endoplasmic reticulum (ER), Golgi complex, and endo-lysosomal system—at all times. To date, the cellular mechanisms responsible for this type of coordination remain poorly understood.

In this study, we focus on the first steps in the pathway; namely, the folding and export of secretory cargo from the ER. Here, the fluctuations in protein synthesis that may occur in many cell types (Dolfi et al., 2013; Ron and Harding, 2012; van Anken et al., 2003) could lead to aberrant accumulation of folded and potentially active cargo in the lumen of this this organelle, with harmful consequences for the cell or organism. Examples of cargo mislocalization and anomalous activation at the ER, leading to diseases such as cancer, have been reported (Choudhary et al., 2009). Thus, the production of folded cargo proteins in the ER must be coupled with the export process by a mechanism that senses folded cargo and regulates cargo export and synthesis accordingly.

To unravel the expected coordinating mechanism, we developed a strategy based on exposing the ER to a suitable (specific and non-toxic) artificial perturbation designed to induce a synchronous increase of folded cargo in the ER lumen (or "folding pulse" for brevity). This cargo increase should be detected by a sensor in the ER and activate a molecular cascade that would result in accelerating cargo export to decrease the cargo overload (Figure S1A). Such an auto-regulatory cascade is likely to involve signaling pathways because the acute regulation of

most cellular functions, including membrane transport, is mediated by signaling networks (Cancino et al., 2014; Farhan et al., 2010; Giannotta et al., 2012; Pulvirenti et al., 2008). We therefore used a targeted phosphoproteomics approach to detect the phosphorylation of signaling components induced by the folding pulse because these components might then lead to the identification of the complete auto-regulatory device.

We find that an ER auto-regulatory system indeed exists and operates through a surprisingly complex set of molecular reactions at the (ER exit sites) ERESs. Sec24, the cargo-recruiting subunit of the coatomer protein II (COPII) coat-mediated ER export machinery (Barlowe and Helenius, 2016; Mancias and Goldberg, 2008; Miller et al., 2003), doubles as a cargo sensor and, upon binding folded cargo, acts as a guanine nucleotide exchange factor (GEF) to activate the signaling protein Gα12. Gα12, in turn, activates multiple signaling cascades. These signals activate and orchestrate a series of molecular events responsible both for ER export, including packaging of cargo proteins in carriers and fission and translocation of these carriers toward the Golgi, as well as attenuation of protein synthesis, reducing the amount of folded cargo in the ER lumen and preventing accumulation of folded cargo in the ER.

We term this regulatory process AREX (auto-regulation of ER export). Impairment of AREX function results in inefficient secretion and accumulation of cargo in the ER. Furthermore, genetic ablation of key AREX components results in dampened antibody secretory responses, impairment in von Willebrand factor-dependent wound healing mechanisms, and problems regarding the proper formation of bones (Discussion). Thus, defects in AREX proteins are associated with major problems regarding secretion and with pathologies.

RESULTS

Generating a Suitable Perturbation of the ER Export System by Inducing a Cargo Folding Pulse

To generate a suitable perturbation to the ER export machinery, we elicited a synchronous surge of folded cargo in the ER by using temperature-sensitive proteins, such as vesicular stomatitis virus ts045 G protein (referred to hereafter simply as VSV-G) and Pro-Collagen I (PC-I) (Bonfanti et al., 1998; Mironov et al., 2003). VSV-G and PC-I share a critical feature: they do not fold at 40°C and can be accumulated in the ER in the unfolded state at this temperature; when the temperature is then shifted to 32°C, they fold rapidly, generating a surge of folded cargo in the ER (cargo folding pulse) (Bonfanti et al., 1998; Mironov et al., 2003; STAR Methods). This can represent a suitable challenge to the ER export machinery (Aridor et al., 1999; Farhan et al., 2008).

In practice, we accumulated PC-I and VSV-G in the ER in fibroblasts and HeLa cells, respectively, at 40°C for 3 h (STAR Methods). The resulting PC-I levels were severalfold higher than those observed in unperturbed cells, as expected (Figures 1A and 1B). Also, VSV-G markedly accumulated in the ER under similar conditions (Figure 1C). The cells appeared viable after cargo accumulation and exhibited no signs of the unfolded protein response (UPR) (Walter and Ron, 2011), in contrast to cells treated with the UPR activators tunicamycin or thapsigargin and when subjected to specific tests of X-box Protein 1 (XBP1) splicing (Figure S1B) or chaperone GRP78 or BiP increase (Figures S1C and S1D).

We then released the folding block by shifting the temperature to 32°C. Each cargo concentrated within 2–4 min at the ERESs, as determined by co-labeling VSV-G with the COPII coat subunits Sec31A (Figure 1D) and Sec24A (Figure 1E) or PC-I with TANGO-1, a cargo adaptor for collagens (Gorur et al., 2017; Saito et al., 2009; Figure S1F). Both cargos then exited the ER for the Golgi, efficiently bringing back the cargo content of the ER to the steady-state levels within 16 min for both VSV-G (Figure 1F, leftmost image) and PC-I (Figure 1B, third image; Figure S1G, leftmost image). We note that this rapid concentration and exit of VSV-G and PC-I reflects an acceleration of the overall cargo export rates over the export rates at 40°C, when the exportable folded cargo levels are very low (Forster et al., 2006), and that this acceleration is accompanied by an increased flux of carriers out of the ER, as indicated by previous studies (Aridor et al., 1999; Farhan et al., 2008) as well as by data presented later (see below).

The Cargo Folding Pulse Triggers a Signaling Response

To unravel the molecular basis of this adaptive acceleration of export, we sought to identify the expected signaling response to the surge of folded cargo. To this end, we used a targeted phosphoproteomics approach to assess the phosphorylation state of several hundred kinases and regulatory proteins within 4 min after the temperature shift, when cargo engages the export machinery. Remarkably, both VSV-G and PC-I folding induced phosphorylation changes in a subset of proteins at specific regulatory residues (83 proteins for VSV-G and 73 proteins for PC-I; Table S1). Analysis of these data using bioinformatics tools and manual curation delineated a number of known signaling pathways. The most enriched pathways were activated by both cargoes and were involved in G-protein-cyclic AMP (cAMP)-protein kinase A (PKA) signaling, regulation of protein synthesis, and mitogenic signaling (Figures 2A and S1H). Western blot experiments confirmed the phosphorylation and activation of the key kinase components of these pathways, as judged by phosphorylation of PKA regulatory subunit IIa (PKA-RIIa) and of many PKA substrates (Figure 2B), of PKR and eIF2α (Figure 2C), and of ERK1 or ERK2 or Akt (Figure 2D). A difference between VSV-G and PC-I was that the former induced the activation of ERK1 or 2 but not of Akt, whereas the latter activated Akt but ERK1 or 2 phosphorylation was unchanged (Figure 2D).

These signaling responses were not influenced by temperature shifts or cycloheximide treatment and were dependent on the degree of expression of VSV-G or PC-I (Figures S1I and S1J). As a further control, we used the transmembrane cargo protein E-Cadherin engineered with a hook-and-release system (retention using selective hooks [RUSH], hereafter called streptavidin binding protein (SBP)-mCherry-E-Cadherin or SBP-EGFP-E-Cadherin), which can be trapped and accumulated in a temperature-independent fashion in a segregated domain of the ER and then released to engage the export machinery by addition of biotin (Boncompain et al., 2012). E-cadherin, like VSV-G, was expected to interact with COPII via its D-X-E-containing cytosolic tail (Mancias and Goldberg, 2008; Nishimura

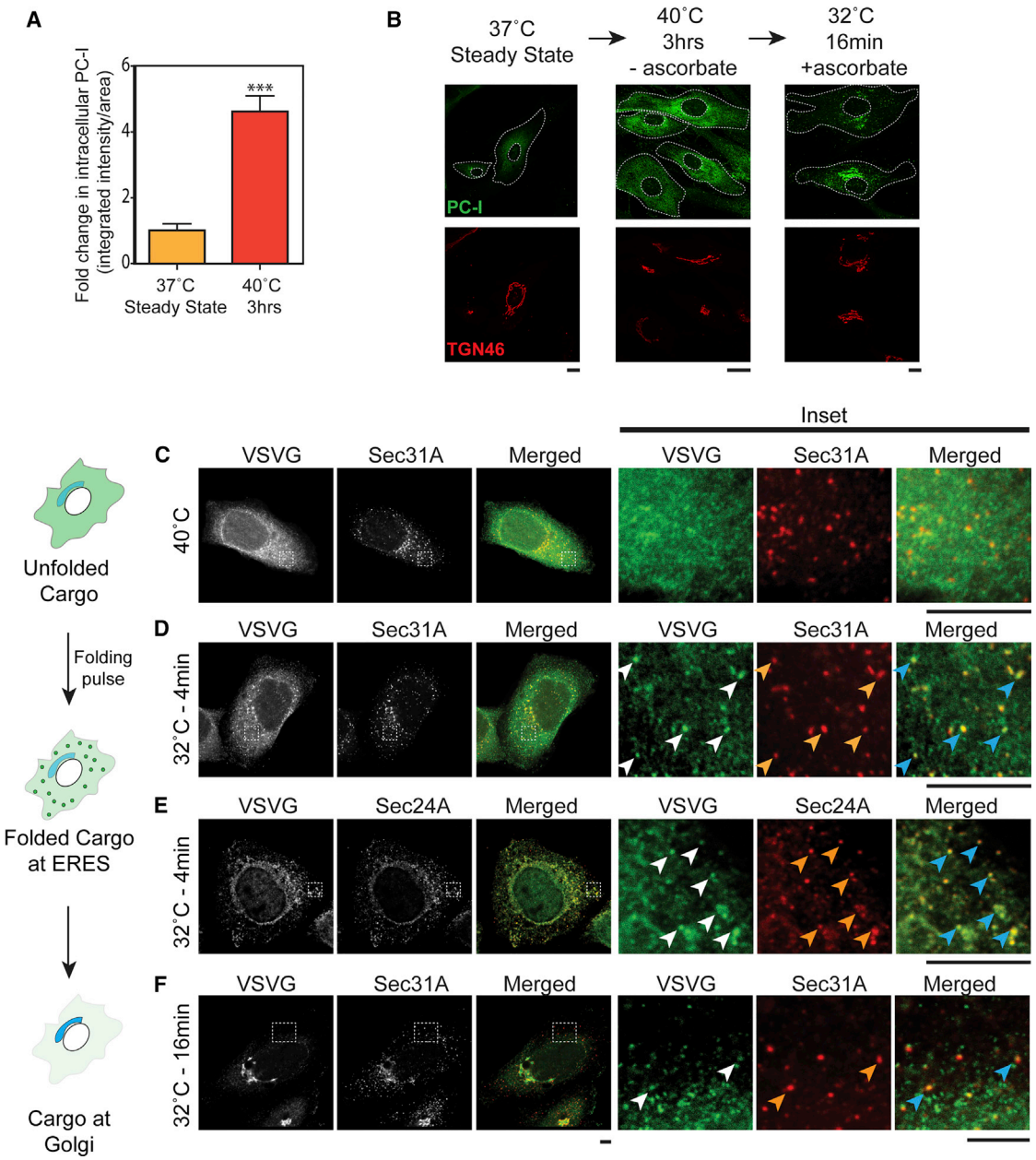

Figure 1. A Surge of Folded Cargo in the ER Concentrates at the ERESs Before Export to the Golgi

(A) Fold change in intracellular immunofluorescence (IF) staining intensity of total PC-I in fibroblasts cultured under folding block conditions and normalized to unperturbed human fibroblasts (n = 22 cells). Data represent mean ± SEM. The p values were calculated by Student's t test; ***$p < 0.001$.

(B) IF staining of PC-I and a Golgi marker (TGN46) in primary human fibroblasts under steady-state, folding block, and transport pulse conditions. Scale bar, 20 μm.

(C–F) IF staining of VSV-G and ERES markers in HeLa cells infected with ts045 VSV-G and (C) cultured at 40°C for 3 h and (D and E) shifted to 32°C for 4 min, and (F) to 32°C for 16 min. Arrowheads indicate colocalizing puncta. Cells were treated with cycloheximide for 30 min before folding or transport pulses. Scale bars, 10 μm.

and Balch, 1997) and exhibited similar behaviors of ER export and signaling responses (Figures S1K and S1L).

In conclusion, a synchronous increase in folded cargo in the ER initiates a signaling network similar in complexity and intensity to those elicited by plasma membrane receptors (Wong and Scott, 2004).

The Cargo-Activated Signaling Pathways Enhance Cargo Export and Inhibit Protein Synthesis

According to the ER auto-regulation hypothesis, some of these pathways should activate export or inhibit cargo synthesis to counteract the ER overload. We tested this hypothesis by inhibiting the core kinases in these pathways (STAR Methods).

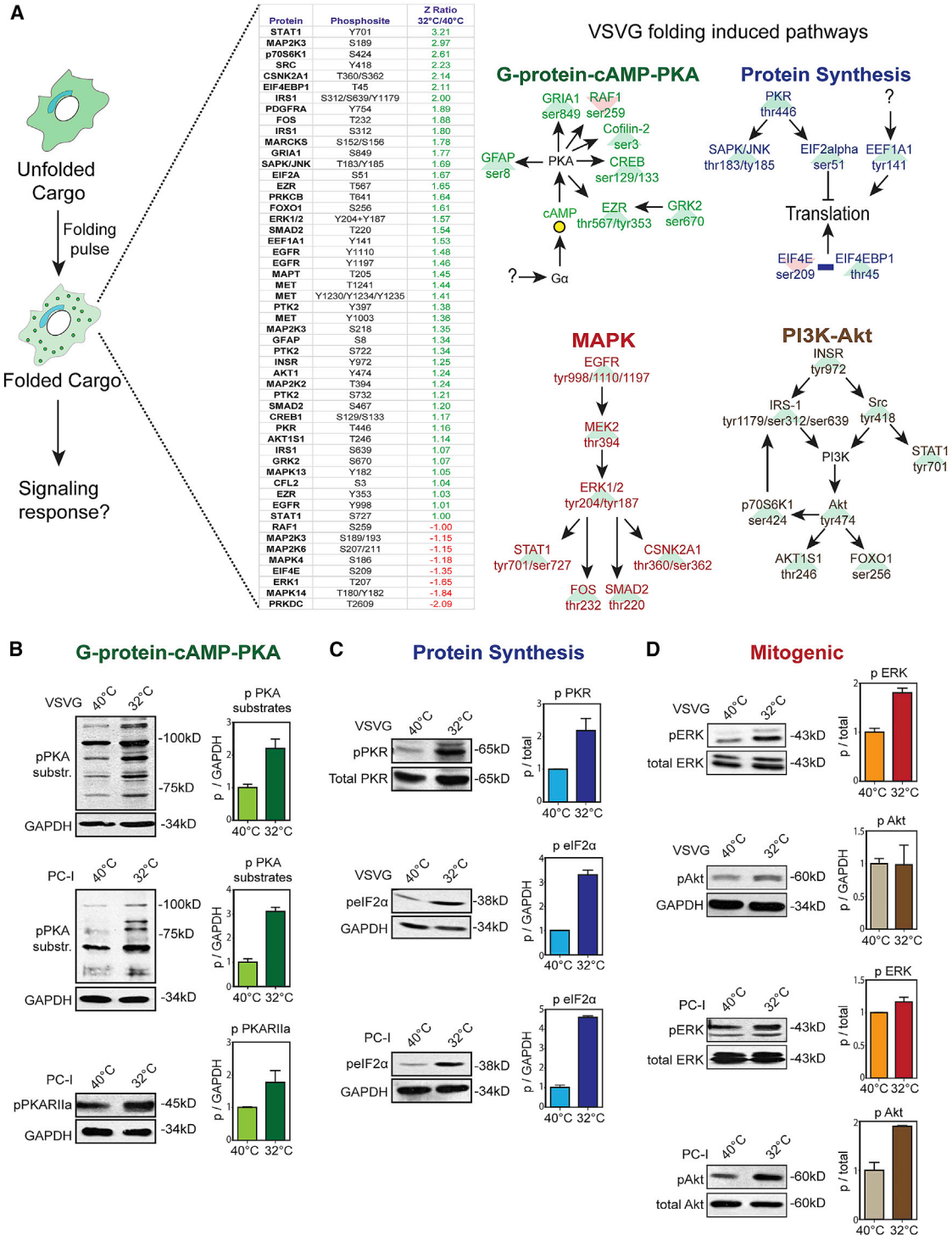

Protein	Phosphosite	Z Ratio 32°C/40°C
STAT1	Y701	3.21
MAP2K3	S189	2.97
p70S6K1	S424	2.61
SRC	Y418	2.23
CSNK2A1	T360/S362	2.14
EIF4EBP1	T45	2.11
IRS1	S312/S639/Y1179	2.00
PDGFRA	Y754	1.89
FOS	T232	1.88
IRS1	S312	1.80
MARCKS	S152/S156	1.78
GRIA1	S849	1.77
SAPK/JNK	T183/Y185	1.69
EIF2A	S51	1.67
EZR	T567	1.65
PRKCB	T641	1.64
FOXO1	S256	1.61
ERK1/2	Y204+Y187	1.57
SMAD2	T220	1.54
EEF1A1	Y141	1.53
EGFR	Y1110	1.48
EGFR	Y1197	1.46
MAPT	T205	1.45
MET	T1241	1.44
MET	Y1230/Y1234/Y1235	1.41
PTK2	Y397	1.38
MET	Y1003	1.36
MAP2K3	S218	1.35
GFAP	S8	1.34
PTK2	S722	1.34
INSR	Y972	1.25
AKT1	Y474	1.24
MAP2K2	T394	1.24
PTK2	S732	1.21
SMAD2	S467	1.20
CREB1	S129/S133	1.17
PKR	T446	1.16
AKT1S1	T246	1.14
IRS1	S639	1.07
GRK2	S670	1.07
MAPK13	Y182	1.05
CFL2	S3	1.04
EZR	Y353	1.03
EGFR	Y998	1.01
STAT1	S727	1.00
RAF1	S259	-1.00
MAP2K3	S189/193	-1.15
MAP2K6	S207/211	-1.15
MAPK4	S186	-1.18
EIF4E	S209	-1.35
ERK1	T207	-1.65
MAPK14	T180/Y182	-1.84
PRKDC	T2609	-2.09

Figure 2. Cargo Folding Activates Multiple Signaling Pathways

(A) Schematic of the targeted phosphoproteomics analysis during a VSV-G folding pulse. A representative subset of proteins were mapped into enriched signaling pathways and connected by arrows (see Table S1 for a full list).

(B–D) Western blot analyses of the (B) PKA substrate phosphorylation pattern (100 kD to 50 kD) and PKA-RIIa (Ser99) phosphorylation, (C) PKR (Thr446) and eIF2α phosphorylation (Ser51), and (D) ERK1 or ERK2 (Thr202/Tyr204) and Akt (Ser473) phosphorylation under cargo folding block (40°C) and folding pulse (32°C – 4 min). Histograms (mean ± SEM) correspond to fold change in signal intensity after the cargo folding pulse normalized to intensity under folding block conditions.

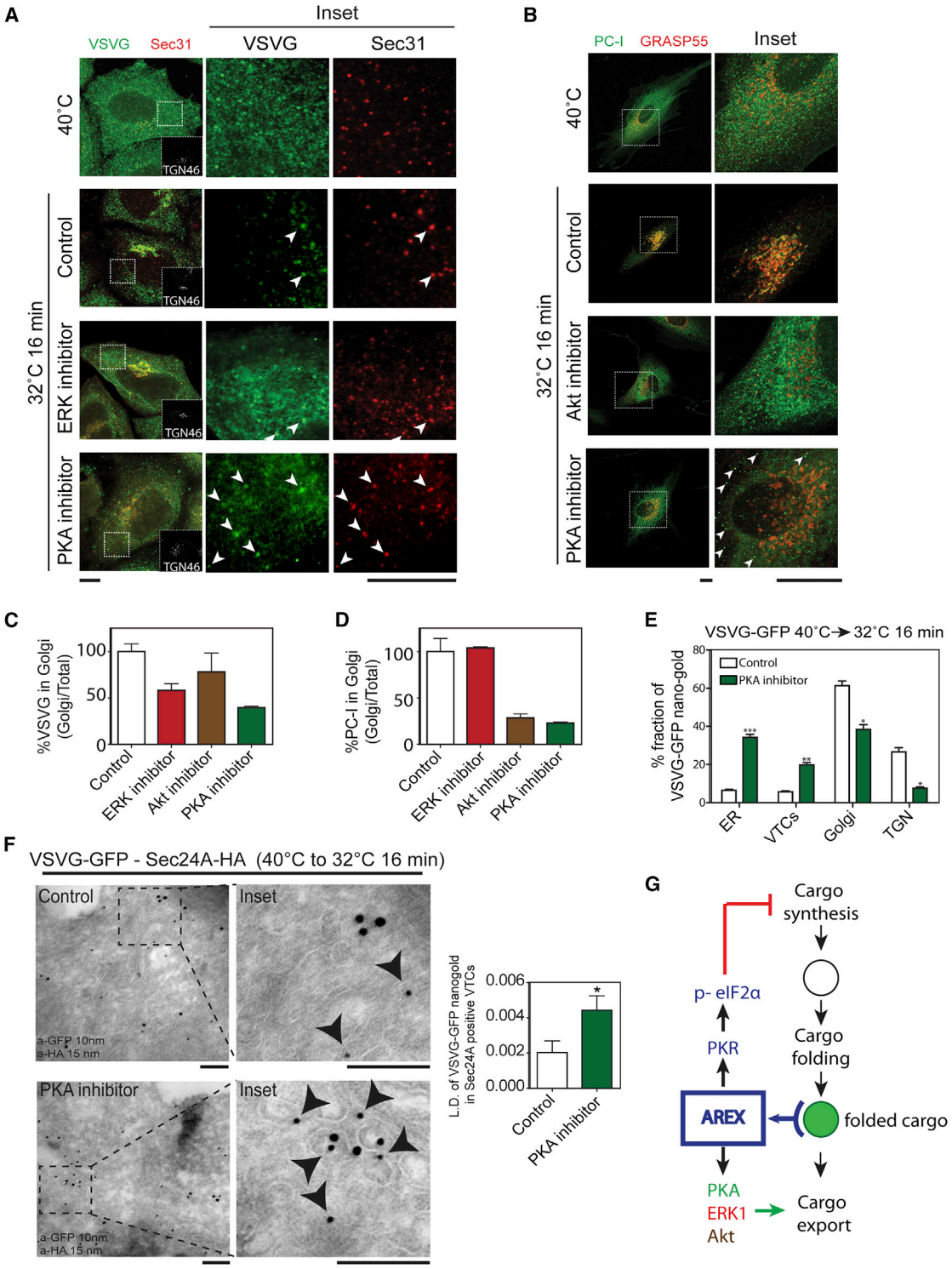

Figure 3. The Cargo-Activated Kinases Are Required for Cargo Export from the ER

(A) IF staining for VSV-G, Sec31A, and TGN46 in cells treated with the control (DMSO) or PKA (PKI-1422), or ERK (PD98059) inhibitors after a cargo transport pulse. White arrowheads indicate cargo and Sec31A-colocalizing puncta. Scale bars, 10 μm.

(B) IF staining for PC-I and GRASP55 after a cargo transport pulse in cells treated with the control (DMSO) or Akt (FPA-124) or PKA (PKI-1422) inhibitors. Scale bars, 10 μm.

(legend continued on next page)

The PKA Pathway

Blocking PKA activity strongly suppressed the ER export of VSV-G, PC-I, and E-Cadherin (Figures 3A–3D; Figures S2A–S2C; Videos S1 and S2). Importantly, we determined that PKA inhibition or PKA-RIIa depletion does not affect COPII assembly and the concentration of folded cargoes at the ERESs, consistent with previous reports (Lee and Linstedt, 2000); at the same time, it does inhibit ER export by blocking the exit of concentrated cargo from the ERESs (Figures 3A, 3B, and S2B, fourth rows, white arrowheads; Videos S1 and S2). Immunoelectron microscopy confirmed that, upon PKA inhibition, VSV-G concentrates in vesicular tubular clusters (VTCs) apparently budding from ER elements (marked by the COPII coat protein Sec24A) but does not leave the exit sites and does not efficiently reach the Golgi (Figures 3E and 3F). Thus, PKA is required for a late stage in the ER export process; i.e., apparently for the uncoating and separation of cargo-laden VTC membranes from the ER.

The Mitogenic Pathways

Here inhibition of ERK activity or depletion of ERK1 moderately retarded the ER export of VSV-G (Figures 3C, S2C, and S2D), with the fraction of VSV-G left in the ER appearing diffuse and poorly recruited to ERESs (Figures 3A and S2B, third rows), consistent with the reported effect of the kinase on Sec16 and the regulation of ERES numbers (Farhan et al., 2010). PC-I export in fibroblasts, instead, was not detectably affected by ERK inhibition (Figure 3D). In contrast, Akt inhibition substantially blocked PC-I transport to the Golgi, resulting in diffuse distribution of PC-I in the ER, but had no clear effect on VSV-G transport (Figures 3B, third row, 3C, and 3D). Thus, the mitogenic kinases act on an early export step; i.e., concentration of cargo at the ERESs.

The PKR- eIF2α Pathway

Depletion of PKR by small interfering RNA (siRNA) did not affect the ER-to-Golgi transport of VSV-G (Figure S2E) or PC-I (data not shown). PKR, a member of the eIF2α kinase family, is activated by multiple stress stimuli to induce eIF2α phosphorylation at serine 51, which inhibits protein synthesis (Pakos-Zebrucka et al., 2016). We therefore tested the role of PKR in cargo-induced phosphorylation of eIF2α by depleting PKR and assaying for phospho-eIF2α during a folding pulse. As a control, we also depleted the related UPR eIF2α kinase PERK (Walter and Ron, 2011). At 40°C, eIF2α phosphorylation was not affected (Figure S2F) in both control and depleted cells, suggesting that both PKR and PERK were inactive under this condition. Upon cargo folding at 32°C, the increase in eIF2α phosphorylation was inhibited in PKR-depleted but not in PERK-depleted cells, indicating that PKR is the mediator of eIF2α phosphorylation induced by folded cargo (Figures S2F and S2G).

Altogether, these results are in accord with the auto-regulation model, by which increases in folded cargo should generate signals that act to reduce the ER cargo load. We call this regulatory process AREX (see Figure 3G for a schematic).

Molecular Composition and Organization of the AREX Signaling Pathways

To study the molecular make-up of the signaling pathways activated by cargo, given the robust and general role of PKA in ER export, we considered that AKAP (A kinase-anchoring protein) scaffold-based signaling complexes may provide a suitable model. AKAPs are scaffolds that anchor PKA-dependent pathways and other regulatory proteins onto specific cellular structures, often forming large signaling complexes (Scott et al., 2013; Taylor et al., 2008; Wong and Scott, 2004). To elucidate the specific components and organization of the AKAP-based AREX signaling system, we used a series of concatenated folding pulse experiments.

Cargo Folding Activates and Recruits PKA at the ERESs

PKA is comprised of homo-dimers of catalytic and regulatory subunits. The latter bind to a conserved motif in the AKAPs and are activated upon binding cAMP (Carr et al., 1992; Scott et al., 2013), which is followed by detachment of the catalytic subunits (Cancino et al., 2014; Taylor et al., 2008). We found that, in cells kept at 40°C to accumulate unfolded cargo, PKA does not reside at the ERESs; the regulatory subunit PKA-RIIa localizes mainly in an uncharacterized cluster of perinuclear puncta that does not co-stain for the ERES marker Sec31A (Figure 4A, left) and the catalytic subunit PKA-Cα shows a diffuse distribution (Figure S3A, left). Then, upon induction of the cargo folding pulse, both PKA-RIIa and PKA-Cα were recruited selectively to the sub-population of the ERESs where VSV-G concentrated (Figures 4A and S3A, right, white arrowheads). At the same time, cAMP increased in various peripheral regions of the cytoplasm of cells, as detected by an EPAC fluorescence resonance energy transfer (FRET)-based probe, consistent with an adenylate cyclase being activated in the ER (Figure 4B).

Examining PKA-dependent phosphorylation by western blotting with a characterized antibody against PKA-phosphorylated substrates, we found a markedly enhanced overall phosphorylation pattern during a folding pulse, with several major phospho-PKA substrate bands being stronger and some unchanged compared with the pattern in cargo-containing cells kept at 40°C (Figure 4C).

(C and D) Percentage of ER-to-Golgi transport of (C) VSV-G (n = 100–150 cells) and (D) PC-I (n = 50 cells) in cells pre-treated for 60 min with inhibitors of PKA (PKI-1422, 100 μM), ERK1 or ERK2 (PD98059, 25 μM), and Akt (FPA-124, 10 μM) and normalized to the control (DMSO). Histograms represent mean ± SEM.

(E) VSV-G-GFP subjected to an ER-to-Golgi transport pulse under control or PKA inhibitor treatments and processed for cryo-immunogold labeling. GFP (10 nm) in organelles and profiles were counted and segregated by ultrastructure into the ER, vesicular tubular clusters (VTCs), the Golgi, and the *trans*-Golgi network (TGN) (n = 19 cells for control; n = 26 cells for PKI-1422). The data represent the mean ± SD. The p values were calculated by Student's t test; *$p < 0.05$, **$p < 0.01$, ***$p < 0.001$.

(F) VSV-G-GFP subjected to an ER-to-Golgi transport pulse under control or PKA inhibitor (PKI-1422, 100 μM) treatment and processed for cryo-immunogold labeling for GFP (10 nm) and Sec24A-HA (15 nm). Arrowheads mark the cargo in the ERESs or VTCs. Scale bars, 150 nm. VSV-G-GFP in Sec24A-positive VTCs under control (n = 45 VTCs) or PKA inhibitor (n = 103 VTCs) conditions is plotted as a linear density (number of gold particles per nanometer). The p value was calculated by Student's t test; *$p < 0.05$.

(G) Schematic of the AREX signaling cascade. AREX senses folded cargo in the ER and activates export via PKA, ERK, or Akt (green) or inhibits protein synthesis via PKR-mediated phosphorylation of eIF2α (red).

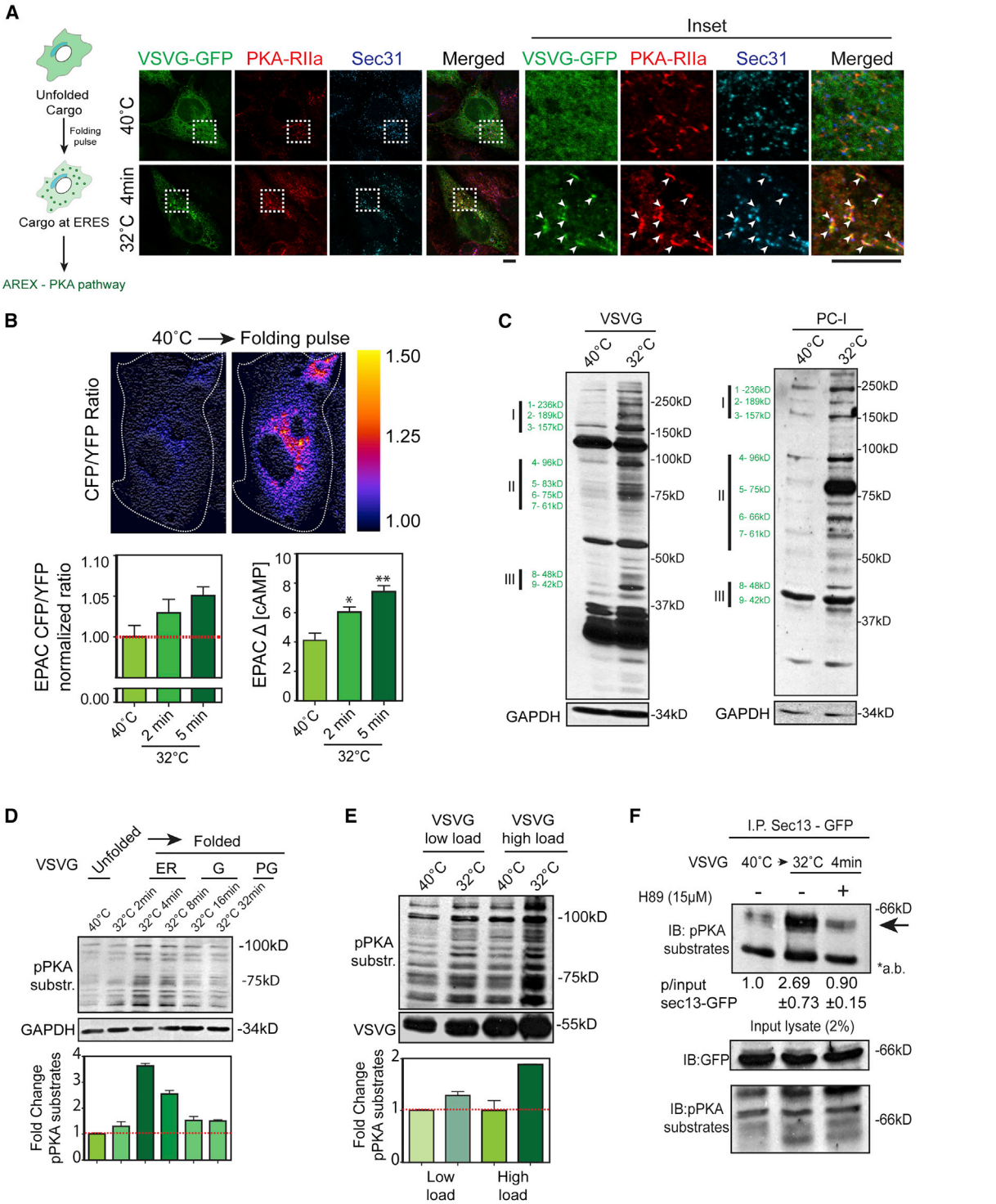

Figure 4. The AREX-PKA Complex Is Recruited and Activated at the ERESs

(A) IF localization of PKA-RIIa and VSV-G-GFP under folding block and folding pulse conditions. Scale bars, 10 μm. White arrowheads indicate colocalizing puncta.

(B) cAMP levels measured in cells after a VSV-G folding pulse relative to the folding block. Representative pseudocolored images of the CFP:yellow fluorescent protein (YFP) FRET ratio (n = 5 independent experiments) are shown. The normalized CFP:YFP ratio and relative cAMP levels were quantified (n = 15–20 cells, mean ± SE). The p values were calculated by Student's t test; *$p < 0.05$, **$p < 0.01$.

(legend continued on next page)

We then carried out similar analyses in unperturbed HeLa cells and human fibroblasts and observed a pattern of PKA localization and substrate phosphorylation intermediate to that seen at 40°C and during a folding pulse (see legends for Figures S3C and S3D).

Characterizing the cargo-induced PKA phosphorylation response further, we found that (1) the intensity of phosphorylation decreased over time, in parallel with the decrease of folded cargo in the ER (Figure 4D); (2) the intensity of phosphorylation was proportional to the amount of cargo in the ER during the pulse (Figure 4E); (3) one of the substrates phosphorylated by PKA was Sec13, a COPII coat subunit (Figures 4F, S3E, and S3F); and (4) the phosphorylation of substrates induced by an unrelated stimulus, such as a β-adrenergic receptor ligand in HeLa cells, was completely different from that induced by AREX and did not include Sec13 (Figures 4F, S3D, and S3G), indicating that the two PKA pathways are segregated from each other, as expected. These results collectively indicated that PKA is activated by cargo folding selectively at the ERES and prompted us to search for other relevant PKA pathway components.

Cargo Folding Activates Gα12 and ADCY7 at the ERESs

The canonical activators of PKA are adenylate cyclases (ADCYs) (Cooper, 2005). In a previous study, we had expressed tagged constructs encoding for the ubiquitous ADCYs (4, 7, and 9) (Cooper, 2005) to determine their subcellular localization (Cancino et al., 2014). We report here that ADCY7 localizes to the ER in unperturbed HeLa cells (Figure S4A). The canonical activator of ADCYs among the different heterotrimeric G-proteins is Gαs (Cooper, 2005; Wettschureck and Offermanns, 2005). However, neither siRNA-mediated knockdown of Gαs nor use of the Gαs minigene exerted detectable effects on ER export (Cancino et al., 2014). Searching for alternative activators, we noted that ADCY7 activity can be stimulated not only by Gαs but also by Gα12 and Gα13 (Jiang et al., 2008). Of these G-proteins, we determined Gα12 to be in part localized to the ERESs (and in part diffuse in the cytosol) in unperturbed HeLa cells (Figure S4B). We thus tested the roles of ADCY7 and Gα12 in the AREX response during a folding pulse by carrying out a series of functional, localization, and molecular interaction experiments.

The results are summarized below and show that ADCY7 and Gα12 are recruited to the ERESs during a folding pulse and are necessary for PKA-dependent activation and ER export of cargo, as indicated by the following evidence. (1) depletion of ADCY7 or Gα12 (Figures S4C–S4E) blocked cargo transport from the ER to the Golgi (Figures 5A–5D, S4F, and S4G); moreover, depletion of ADCY7 or Gα12 prevented cargo folding-induced PKA substrate phosphorylation (Figure S4H). Instead, depletion of Gα13 had no effect (Figures 5B and 5D). The export block was due to a reduced production of cAMP because a membrane-permeant cAMP analog (8 bromo cyclic AMP [8-Br-cAMP]) rescued ER-to-Golgi transport (Figures 5A–5D). (2) Experiments with Gα12 knockout mouse embryonic fibroblasts ($Gna12^{-/-}$ MEFs) gave similar results; ER export of VSV-G was inhibited (Figure 5E, center), and expression of a construct encoding wild-type human Gα12 (Gα12-myc) resuscitated VSV-G export to the Golgi (Figure 5E, right). (3) During the VSV-G folding block, neither ADCY7 nor Gα12 localized at the ERESs. ADCY7, a transmembrane protein, showed an ER-like distribution (Figure 5F, left), and Gα12 was in uncharacterized cytosolic puncta (Figure 5G; left); however, during a folding pulse, both proteins were strikingly recruited to the VSV-G-concentrating ERESs (Figures 5F and 5G, right, arrowheads). (4) Recruitment of Gα12 to the ERESs coincided with the activation of this G-protein, as determined using a construct encoding the tetratricopeptide repeat domain of phosphatase PP5 (TPR-PP5) that binds active Gα12 (Yamaguchi et al., 2003). TPR-PP5 bound to Gα12 (Figure S4I) and was recruited to Gα12 at the ERESs (Figure S4J, red arrows), as shown by both co-immunoprecipitation and imaging experiments. (5) Recruitment of ADCY7 to the ERESs required the presence of Gα12, as shown by Gα12 depletion experiments (Figure S4K). Moreover, activated Gα12 interacted with ADCY7, as shown by experiments where only the constitutively active form of Gα12 (Gα12Q229L, guanosine triphosphate [GTP]-locked) co-immunoprecipitated with ADCY7 (Figure S4L), whereas the inactive form (Gα12G228A, guanosine diphosphate [GDP]-locked) did not, indicating that Gα12 activation is required for ADCY7 recruitment. (6) Overexpression of GDP-locked Gα12 (Gα12G228A) in HeLa cells suppressed VSV-G ER export (Figure S4M, center), whereas overexpression of GTP-locked Gα12 (Gα12Q229L) accelerated VSV-G export, with cargo present both in the Golgi and the plasma membrane 16 min after release from the ER (Figure S4M, right).

Thus, we conclude that Gα12 is recruited and activated by GDP to GTP exchange at the cargo-laden ERESs after folding and then promotes ER export via recruitment and activation of ADCY7.

AKAP-Lbc and PDE3B Are Required for PKA Recruitment to the ERESs and for ER Export

The AKAP scaffolding proteins are major candidates to serve as PKA anchors at the ERESs (Scott et al., 2013; Wong and Scott,

(C) Analyses of the VSV-G and PC-I cargo folding-stimulated PKA substrate phosphorylation pattern. Nine main bands corresponding to molecular weight (*Mw*) ranges of 242,000–162,500 (cluster I), 100,000–60,000 (cluster II), and 47,500–42,000 (cluster III) are marked next to each cargo. The approximate *Mw* was calculated using the Dual Color Plus standard protein marker as an internal reference within an experimental error of ± 8,000 Da. The pattern of bands was similar for both cargoes but not the same regarding differences in the intensity of phosphorylation of some bands.

(D) PKA substrate phosphorylation pattern (100 kD to 50 kD) in HeLa cells up to 32 min after VSV-G folding pulse. ER, endoplasmic reticulum; G, Golgi; PG, post Golgi. Histograms (mean ± SE) represent the intensity of bands at 100 kD and 75 kD.

(E) PKA substrate phosphorylation pattern in HeLa cells accumulated with ts045 VSV-G virus for 30 min (low load) or 3 h (high load) at 40°C and subjected to a folding pulse. Histograms (mean ± SE) represent the cumulative intensity of bands at 100 kD and 75 kD.

(F) Sec13-GFP immunoprecipitated and probed with the phospho-PKA substrate antibody under VSV-G folding block or folding pulse conditions with or without 15 μM H89, a PKA inhibitor. Densitometric quantification and fold change in pSec13:input Sec13 was calculated, normalized to intensity under folding block (mean ± SEM).

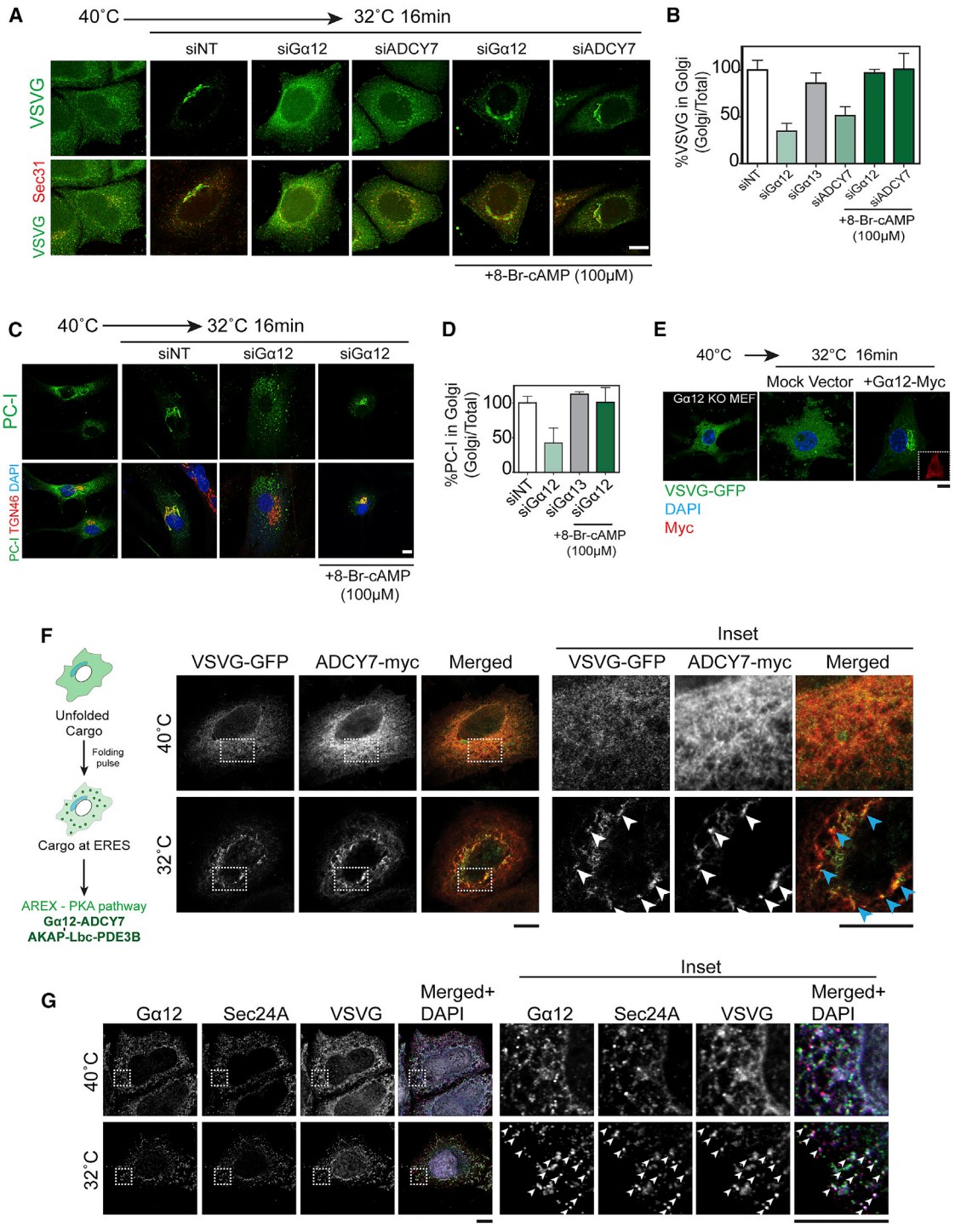

Figure 5. ADCY7 and Gα12 Are Activated and Recruited to the ERES in Response to Cargo Folding and Regulate Cargo Export

(A) IF staining for VSV-G and Sec31A after a transport pulse in cells treated with non-targeting, Gα12 or ADCY7 siRNAs. Scale bars, 10 μm. 100 μM 8-Br-cAMP was added 30 min before the temperature shift to 32°C.

(B) Percentage of ER-to-Golgi transport of VSV-G in cells treated with siRNAs against Gα12, Gα13, or ADCY7 and normalized to the non-targeting siRNA (siNT) control. 100 μM 8-Br-cAMP was added 30 min before the temperature shift to 32°C (n = 50–100 cells, mean ± SEM).

(C) IF staining for PC-I and TGN46 after a transport pulse in cells treated with non-targeting siRNAs or Gα12 siRNAs. Scale bars, 10 μm. 100 μM 8-Br-cAMP was added 30 min before the temperature shift to 32°C.

(legend continued on next page)

2004). We noted that, among these members, AKAP-Lbc (also called AKAP13), a well-characterized AKAP, binds active Gα12 in addition to PKA (Diviani et al., 2001). AKAP-Lbc also anchors phosphodiesterase (PDE) enzymes to confine or terminate PKA activation via cAMP degradation (Scott et al., 2013). We further noted that, among PDEs, PDE3B has been shown to localize to the ER (Omori and Kotera, 2007), a finding confirmed by us (Figures S4N and S4Q), suggesting that this PDE might participate in AREX signaling. We thus tested whether the above proteins might be involved in controlling ER export.

The following series of observations indicates that AKAP-Lbc and PDE3B are indeed required for the localization and activation of PKA at the ERESs and for the ER export of cargo. (1) Depletion of AKAP-Lbc resulted in marked inhibition of cargo export out of the ERESs (Figures 6A–6C). (2) AKAP-Lbc depletion also prevented recruitment of PKA at the ERESs (Figure S4O) and inhibited the cargo folding-dependent activation of PKA (Figure S4H). (3) ER export was also blocked by treatment with the characterized peptide Ht31 (Figure S4P), which mimics the PKA binding motif in all AKAPs and displaces PKA from the AKAPs (Carr et al., 1992; Scott et al., 2013). (4) Replacing the endogenous AKAP-Lbc with a construct lacking the PKA binding domain (AKAP-Lbc-ΔPKA) blocked transport of cargo to the Golgi (Figure 6D). These collective experiments provide conclusive evidence that the effects of PKA in ER export are mediated by direct binding to AKAP-Lbc.

Regarding the PDE involved in AREX signaling, the following observations indicate a role of PDE3B in ER export. (1) Endogenous AKAP-Lbc robustly co-precipitated both PDE3B and PKA-RIIa (Figure 6E). (2) Depletion of AKAP-Lbc resulted in loss of ER localization of PDE3B (Figure S4Q). (3) Inactivating PDE3B with a specific inhibitor, trequinsin hydrochloride (Shafiee-Nick et al., 2017), or by treatment with specific siRNAs reversed the export block caused by Gα12 or ADCY7 depletion (Figures 6F and 6G), presumably by slowing down cAMP degradation at the ERES and, hence, counteracting the impaired cAMP production in these cells (an effect similar to the one induced by 8-Br-cAMP addition; Figures 5A–5D). (4) In contrast, PDE3B inhibition or knockdown did not reverse the block caused due to AKAP-Lbc depletion (Figures 6F and 6G) or the block induced by the peptide inhibitor Ht31 (Figure S4P), presumably because, under these conditions, PKA is no longer recruited and activated by cAMP at the ERESs. These data indicate that PDE3B is a key regulator of the cAMP pool responsible for PKA activation at the ERESs.

Altogether, multiple lines of evidence converge to support a mechanistic model for recruitment and activation of the AREX complex at the ERESs that is summarized in Figure 7G (see below).

AREX Regulates Both Pulsed and Steady-State Traffic

We next examined whether AREX is required only during the cargo pulses or also for basal secretion. When we disabled the AREX system in fibroblasts, we found PC-I to significantly accumulate intracellularly (Figures 6H, 6I, S4R, and S4S). In unperturbed MEFs from Gna12$^{-/-}$ mice, PC-I formed large and numerous aggregates, consistent with impaired export (Figure 6H, 37°C). When a pulse protocol was applied (i.e., the temperature was shifted to 40°C), the PC-I unfolded and assumed a diffuse ER staining pattern (Figure 6H, 40°C) and then, upon shifting the temperature back to 32°C, re-formed large aggregates in the ER that appeared unable to exit (Figure 6H, 32°C, 16 min). Thus, the PC-I ER export machinery is severely impaired in cells depleted of AREX components under both basal and pulse conditions. However, PC-I continued to be secreted into the medium over 24 h (Figure S4R, supernatant), presumably through some form of compensatory mechanism.

A Cargo-Sec24-Gα12 Complex Links Cargo Folding with AREX Signaling

A key remaining issue is the mechanism linking cargo folding with AREX activation at the ERESs. To address it, we used VSV-G as a model cargo. VSV-G and other transmembrane cargo proteins possess diacidic (D-X-E consensus motif) sequences on their cytosolic tails (Nishimura and Balch, 1997) that allow direct interaction with Sec24A and Sec24B (but not with Sec24C and Sec24D) (Mancias and Goldberg, 2008). In the unfolded state, VSV-G remains diffuse in the ER and concentrates in the ERESs only after folding (Figures 1C–1E), where it binds Sec24 through the cytosolic tail (Mancias and Goldberg, 2008; Nishimura et al., 1999). We thus hypothesized that binding of the VSV-G tail to Sec24 might be involved in the activation of AREX signaling.

To test this notion, we used a VSV-G mutant with an A-I-A sequence in place of the D-X-E motif (VSV-G-AXA-GFP) which folds as efficiently in the ER (Nishimura and Balch, 1997) but does not bind to Sec24A or Sec24B (Mancias and Goldberg, 2008; see schematic in Figure S5A). It thus fails to be recruited to the ERESs and exits the ER slowly (Nishimura and Balch, 1997; Nishimura et al., 1999), presumably by passive bulk flow. If VSV-G binding to Sec24 is required for AREX signaling, then VSV-G-AXA-GFP should not elicit the AREX response. Folding of the AXA mutant failed to elicit activation of PKA or PKR, or phosphorylation of eIF2α (Figure S5A).

To further test the role of the VSV-G tail binding to Sec24, we exposed cells loaded with unfolded VSV-G to a characterized peptide containing the exit motif (GQYTDIEMNR, DIE peptide) of the VSV-G tail or to the corresponding A-X-A peptide (GQYTAAAMNR, AAA peptide). The DIE peptide binds Sec24A or Sec24B by making contacts with two positively charged arginine residues (R750 and R752 on Sec24A) in the β sandwich domain of the protein (whereas the AAA peptide does not) (Mancias and Goldberg, 2008). Both the DIE and AAA peptides were coupled to an octa-arginine repeat sequence to render them membrane-permeant (R8-DIE and

(D) Percentage of ER-to-Golgi transport of PC-I in cells treated with a pool of siRNAs against Gα12 or Gα13 and normalized to non-targeting siRNAs. 100 μM 8-Br-cAMP was added 30 min before the temperature shift to 32°C (n = 50–100 cells, mean ± SEM).

(E) IF staining for VSV-G-GFP after a transport pulse in Gα12 knockout MEFs co-transfected with a mock vector or with human Gα12-myc. Scale bars, 10 μm.

(F and G) IF localization of VSV-G and (F) transfected ADCY7-myc or (G) endogenous Gα12 and Sec24A under folding block and folding pulse conditions. Scale bars, 10 μm. White arrowheads indicate colocalizing puncta.

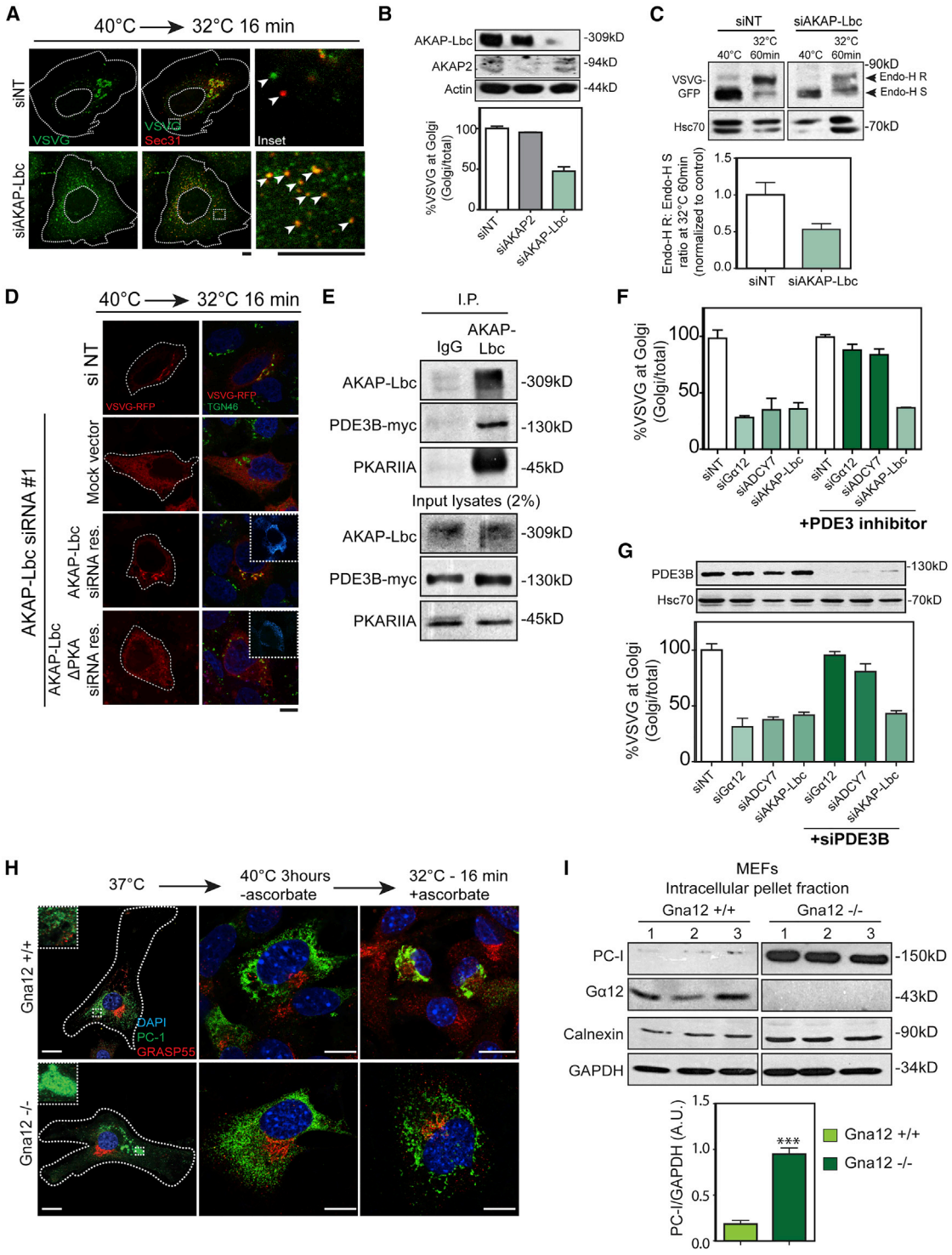

Figure 6. The AREX Cascade Includes AKAP-Lbc and PDE3B as Signaling Components and Is Required for Both Steady-State and Pulsed Traffic

(A) IF staining for VSVG and Sec31A after a transport pulse in cells treated with non-targeting or AKAP-Lbc siRNAs. Scale bars, 5 μm. White arrowheads depict colocalizing puncta.

(B) Percentage of ER-to-Golgi transport of VSVG in cells treated with siRNAs against AKAP-2 or AKAP-Lbc and normalized to non-targeting (siNT) control (n = 50–100 cells, mean ± SEM).

(legend continued on next page)

R8-AAA). R8-DIE triggered the PKA phosphorylation pattern typical of AREX signaling, albeit less efficiently than the full-length VSV-G cargo, whereas R8-AAA had no such effect (Figure S5B). These results further indicated that VSV-G bound to Sec24 initiates AREX signaling.

If this is the case, then Sec24A and Sec24B should be needed for activation of AREX signaling. Indeed, siRNA mediated co-depletion of Sec24A and Sec24B suppressed PKA activation in response to a VSV-G folding pulse (Figure S5C). siRNA mediated co-depletion of Sec24C and Sec24D, however, had no effect on the AREX signaling response (Figure S5C).

Considering that Gα12 is the upstream activator of the AREX cascade (see above), we asked whether the cargo-Sec24 complex might initiate AREX signaling by binding and activating Gα12. To test this notion, we set up a folding pulse experiment and tested for co-immunoprecipitation of VSV-G, Sec24A, and Gα12. Indeed, folded VSV-G (in cells at 32°C after 4 min of shift) reproducibly co-immunoprecipitated with Sec24A and Gα12 whereas unfolded VSVG (at 40°C) did not (Figure 7A). Similar results were obtained using Sec24A as bait (Figure 7B).

We then asked whether cargo-bound Sec24 activates Gα12 by carrying out the co-immunoprecipitation assay with TPR-PP5, an interactor of active Gα12, as bait (Yamaguchi et al., 2003). Sec24A, VSV-G, and Gα12 efficiently co-immunoprecipitated with TPR-PP5 only after triggering the folding pulse (Figure 7C). When cells were co-depleted of Sec24A and Sec24B, a folding pulse failed to induce an increase in Gα12 precipitation by TPR-PP5 (Figure S5D). Collectively, these results suggest that folded VSV-G interacts with Sec24 and the VSVG-Sec24 complex binds and activates Gα12.

We also tested for Gα12 interaction with Sec24 in unperturbed cells because, under these conditions, membrane transport is normally active, and basal activation of the AREX cascade is detectable (Figures S3C and S3D). Sec24A and Sec24B, the mammalian isoforms required for packaging D-X-E cargoes (Mancias and Goldberg, 2008), but not Sec24C and Sec24D, co-immunoprecipitated with Gα12 (Figure S5E). Significantly, upon depleting endogenous cargo in cells with cycloheximide treatment (Forster et al., 2006), we observed reduced co-precipitation of Sec24A with Gα12 (Figure S5F). Thus, unperturbed traffic can support the Sec24-Gα12 interaction, presumably via D-X-E motif-containing endogenous cargo proteins.

To unearth the minimal region on Sec24A that mediates Gα12 binding, we performed a domain truncation analysis. Six main domains can be identified in the three-dimensional crystal structure of Sec24 (Figure 7D) and are highly conserved between Sec24A and Sec24B. Strikingly, only deletion of the Sec24A β sandwich domain (amino acids [aa] 744–828, Δβ/S domain) caused loss of binding to Gα12, whereas individual deletions of all other domains had minimal effects (Figure 7D). Moreover, the isolated β/S domain co-precipitated Gα12 efficiently (Figure S5G). This domain hosts the "B site" of Sec24 that has been shown in yeast to mediate binding to D-X-E motif-bearing cargo proteins (Miller et al., 2003) and, as noted earlier, to contain the binding groove for the DIE motif in VSV-G (Mancias and Goldberg, 2008), suggesting that the VSV-G tail binding to the β/S domain might contribute to the process by which a cargo-Sec24A or Sec24B complex activates Gα12.

To test this model *in vitro*, we examined the activation of Gα12 by the cargo tail-Sec24 complex using tagged proteins isolated by immuno-affinity purification in two independent assays of GEF activity (STAR Methods). In the first assay, active Gα12 was detected by pull-down of a recombinant GST-TPR-PP5 protein (Yamaguchi et al., 2003). Indeed, GST-TPR-PP5 co-precipitated active Gα12 in the presence of Sec24A, GTP-γS, and the R8-DIE peptide but not in the presence of the R8-AAA peptide (Figure 7E). In the second assay, based on the incorporation of GTP-γS^{35} into Gα12, Sec24A likewise stimulated GTP-γS^{35} incorporation in the presence of the R8-DIE but not the R8-AAA peptide (Figure 7F). These data indicate that Sec24, in complex with the VSV-G D-X-E-containing cytosolic tail, can activate Gα12.

Finally, we examined whether these results are consistent with the available knowledge of the crystal structure of Sec24A in complex with Sec23A, Sec22B, and the VSV-G D-X-E tail peptide (aa 502–508 on the VSV-G cytosolic tail [VSV-Gct] (PDB: 3EGD; Mancias and Goldberg, 2008) and the crystal structure of GDP-bound Gα12 (PDB: 1ZCA; Kreutz et al., 2006). Indeed, the predicted supramolecular complex is consistent with our experimental findings (see the legends for Figures S5H–S5J for a description of the model).

Collectively, these results indicate that binding of the D-X-E cargo motif to the β sandwich domain in Sec24A or Sec24B confers to the latter the property to bind and activate Gα12, propagating the AREX signaling cascade (Figure 7G).

(C) ER to Golgi transport of VSVG-GFP in cells treated with siRNAs against AKAP-Lbc as assessed by the Endo-H sensitivity assay. The western blot images are representative of 3 independent replicates. Arrows indicate the Endo-H resistant (Endo-H R) Golgi processed, or Endo-H sensitive (Endo-H S) ER-trapped, bands. The ratio between Endo-H R and Endo-H S bands is indicative of the efficiency in ER export. The ratios between bands at 32°C for 60 min, normalized to non-targeting (siNT) control (mean ± SEM; n = 3) are quantified in the accompanying histogram.

(D) ER to Golgi transport of VSVG-RFP in HeLa cells depleted for AKAP-Lbc (siRNA#1) and co-transfected with AKAP-Lbc-FLAG or AKAP-Lbc-FLAG ΔPKA siRNA resistant constructs. FLAG (inset; cyan); Golgi marker TGN46 (green). Scale bar, 10μm.

(E) Endogenous AKAP-Lbc immunoprecipitated from HeLa cells transfected with myc-tagged PDE3B, followed by western blotting with antibodies against the indicated proteins.

(F and G) Percentage ER to Golgi transport of VSVG, normalized to control (siNT), in cells under Gα12, ADCY7 or AKAP-Lbc depletion and (F) treated with PDE3 inhibitor (n=50 cells) or (G) co-depleted with PDE3B (n=30 cells). Histograms represent mean ± SEM.

(H) IF staining of PC-I and GRASP55 in Gna12+/+ and Gna12-/- MEFs under steady state, folding block and transport pulse conditions. Scale bars, 10 μm.

(I) Western blotting of PC-I, Gα12, ER marker calnexin and GAPDH in the pellet fraction of Gna12+/+ and Gna12-/- MEFs cultured at 37°C. Densitometric quantification of PC-I in WT and Gα12 knockout MEFs normalized to GAPDH (n= 3; data represent mean ± standard error of the mean). p-values were calculated by Student's t-test; ***p <0.001).

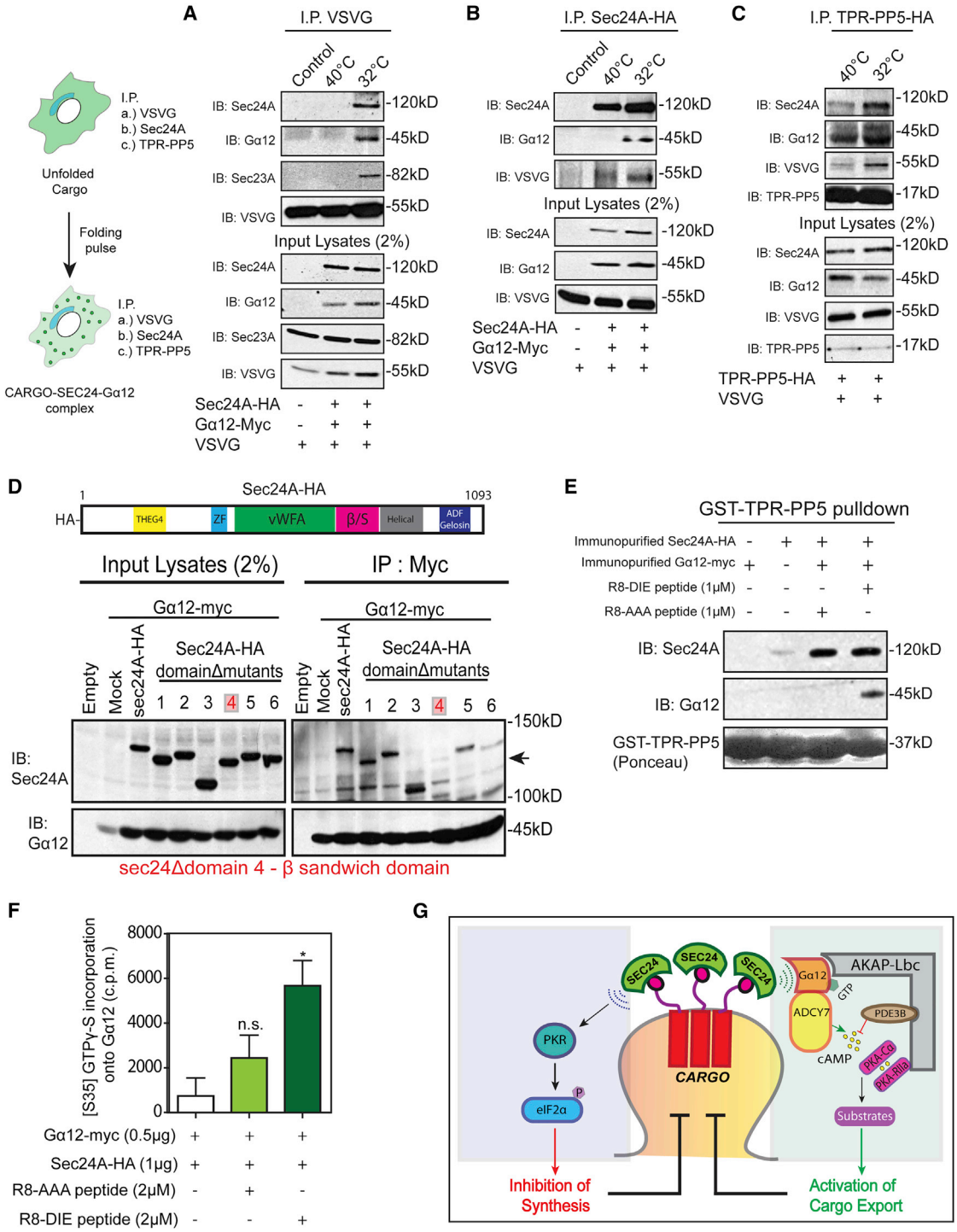

Figure 7. Gα12 Is Recruited and Activated at the ERES by Sec24 in Complex with Cargo

(A–C) Co-immunoprecipitation of VSV-G, Sec24A, and Gα12 under cargo folding block and folding pulse conditions with (A) VSV-G, (B) Sec24A-HA, and (C) TPR-PP5-HA utilized as baits.

(D) Wild-type or domain truncation mutants of Sec24A-HA co-transfected with Gα12-myc and subjected to immunoprecipitation.

(E) *In vitro* GST-TPR-PP5 pull-down of immuno-isolated and affinity-purified Gα12-myc (~1 μg) from reaction mixtures containing Gα12-myc, GDP, GTP-γS, immuno-isolated Sec24A-HA (~1 μg), and either R8-AAA or R8-DIE peptide (1 μM).

(legend continued on next page)

Activation of the AREX PKA Pathway Accelerates Formation of ER Export Carriers

Having outlined the composition of the AREX complex, we asked whether activation of the AREX PKA pathway increases the formation of ER export carriers. Indeed, activation of the AREX PKA pathway by inhibition of PDE3 at the ER (1) enhanced secretion of the bulk flow transport reporter VSV-G-AXA-GFP (Figures S6A–S6C) and (2) increased the surface area or volume of the Golgi stack (Figures S6D–S6G), suggesting an acceleration in the output of membrane carriers from the ER.

AREX Signaling Controls Only a Fraction of the Secretome

Finally, we asked whether AREX controls the secretion of all or just some cargoes. By performing radioactive pulse-chase secretome analyses in HeLa cells (Figure S6H) and also independently monitoring the secretion of a human growth hormone cargo construct (hGH-FM-GFP) whose transport can be synchronized (Gordon et al., 2010; Figures S6I–S6L), we determined that AREX signaling does not control the secretion of all cargo proteins, including hGH-FM-GFP, and affects only a fraction, albeit a significant one, of the secretome.

DISCUSSION

The main finding of this study is that the ERESs are endowed with an auto-regulatory molecular device, the AREX complex, which is activated by the binding of folded cargo to the COPII subunit Sec24. Sec24 acts as a cargo sensor and signal transducer and, upon cargo binding, induces AREX assembly through sequential recruitment and activation of a set of signaling components that include the guanosine triphosphatase (GTPase) Gα12, AKAP-Lbc, and multiple kinases, which then act to modulate cargo export and synthesis as a function of the load of folded cargo in the ER. The AREX assembly sequence is quite complex and is discussed in detail and schematized in Figure S7A.

The main function of AREX is to prevent harmful build-up of folded and potentially active cargo proteins in the ER. This is achieved by monitoring the levels of exportable folded cargo in the ER lumen and co-ordinately executing two control actions: activation of the ER export machineries and attenuation of protein synthesis, both of which contribute to the final effect (Figure 7G). Thus, AREX can be modeled as a control device (Doyle et al., 1992) operating in a sequential multi-step system such as the secretory process to maintain folded cargo in the ER at steady and low levels (see Figure S7B and the legend for a description). The AREX design is analogous to devices used to regulate multi-step manufacturing systems and can be described using the mathematical tools of control theory (Figure S7B; STAR Methods). This suggests that control theory applied to manufacturing plants can be a useful paradigm for future investigations of the biosynthetic system.

Importantly, the AREX system is not a universal regulator of cargo export. It is activated directly by the interaction between cargo proteins containing the D-X-E-motif in their cytosolic tail and the Sec24A or Sec24B isoforms (Figure 7) and regulates the secretion of a subset of cargoes (which include VSV-G, PC-I, and E-Cadherin; Figures 3A–3D, 5A–5D, 6H, 6I, S2A, and S4F). However, a large fraction of the secretome does not require AREX for export. A specific example is the hGH (Figures S6H and S6I). The growth hormone and, in general, AREX-independent cargo proteins are thus expected to activate different signaling pathways to exit the ER. There are four mammalian Sec24 isoforms, each having three potential binding sites for different cargoes or cargo adaptor proteins (Barlowe and Helenius, 2016; Ma et al., 2017; Mancias and Goldberg, 2008; Miller et al., 2003). Some of these sites might be involved in different cargo-dependent signaling reactions. A possible example is the response to folded and accumulated viral proteins described in 1995, which generates calcium and oxygen radicals (ER overload response [EOR]) (Pahl and Baeuerle, 1997). These observations delineate a complex and potentially important territory for future exploration.

Significantly, AREX plays multiple roles in animal physiology. This is evidenced by knockout mouse models indicating that defects in the AREX machinery contribute to pathological states. Adcy7$^{+/-}$ and Gna12$^{-/-}$ mice exhibit weakened antibody secretory responses when challenged with antigens (Duan et al., 2010; Lee et al., 2008). Our study determined that PC-I secretion in Gna12$^{-/-}$ MEFs is significantly impaired (Figures 6H and 6I). Gna12$^{-/-}$ mice, when wounded, have reduced thrombus formation because of the defective secretion of von Willebrand factor (Rusu et al., 2014). Akap13$^{+/-}$ mice display gross defects in bone mineral density and bone volume (Koide et al., 2015), whereas pancreatic islet cells isolated from Pde3b$^{-/-}$ mice exhibit increased insulin secretory responses upon stimulation with glucose (Choi et al., 2006). Thus, knockout mice lacking AREX components exhibit phenotypes that largely correlate with secretion defects. Given that some AREX signaling components are druggable, it might now become possible to pharmacologically modulate the biosynthetic apparatus and the secretome of cells, an area that so far has been poorly exploited for therapeutic purposes.

STAR★METHODS

Detailed methods are provided in the online version of this paper and include the following:

- KEY RESOURCES TABLE
- CONTACT FOR REAGENT AND RESOURCE SHARING
- EXPERIMENTAL MODEL AND SUBJECT DETAILS
  - Cell lines

(F) Radioactive GTP-γS35 incorporation onto immuno-isolated and affinity-purified Gα12-myc (0.5 μg) in the absence or presence of affinity-purified Sec24A-HA (1 μg) and R8-AAA or R8-DIE peptides (2 μM). N = 3 independent replicates; data represent mean ± SEM. The p value comparing absence of peptide with presence of R8-AAA or R8-DIE peptide was calculated by Student's t test; *p < 0.05; n.s., not significant.
(G) Schematic of the AREX signaling complex assembled and activated by folded cargo fluctuations in the ER.

SUPPLEMENTAL INFORMATION

Supplemental Information can be found with this article online at https://doi.org/10.1016/j.cell.2019.01.035.

ACKNOWLEDGMENTS

We thank all members of the A.L. lab for critical evaluation and discussion of the data. We thank Nina Dathan and Daniela Spano for help with cloning and construct preparation. A.L. acknowledges financial support from the Italian Cystic Fibrosis Research Foundation (Project #6), AIRC (Projects IG 15767 and IG 20786), MIUR (Project "FaReBio di Qualità"), the Italian Node of Euro-Bioimaging (Preparatory Phase II – INFRADEV), TERABIO, and the CNR (PON Project 01/00117 and Projects 01-00862 and a3-00025). We thank the Bioimaging Facility of the IBP for help with EM preparation and image acquisition.

AUTHOR CONTRIBUTIONS

Conceptualization, A.L., A.S., and A.C.; Methodology, A.S., A.C., C.d.V., L.G., J.C., S.P., F.F., M.S., and A.L.; Investigation, A.S., A.C., N.R.I., R.R., A.d.C., R.D.M., G.T., M.P., J.C., S.P., F.F., M.S., and A.L.; Formal Analysis, A.S., A.Y., C.d.V., L.G., M.L.M., A.R.B., F.F., and A.L.; Writing – Original Draft, A.S. and A.L.; Writing – Review & Editing, A.S. and A.L.; Visualization, A.S. and A.L.; Funding Acquisition, A.L.; Resources, S.G.K., P.H., and D.D.; Supervision, A.S., C.d.V., L.G., S.P., F.F., M.S., and A.L.

DECLARATION OF INTERESTS

The authors declare no competing interests.

Received: February 27, 2018
Revised: August 30, 2018
Accepted: January 23, 2019
Published: February 28, 2019

REFERENCES

Aridor, M., Bannykh, S.I., Rowe, T., and Balch, W.E. (1999). Cargo can modulate COPII vesicle formation from the endoplasmic reticulum. J. Biol. Chem. *274*, 4389–4399.

Barlowe, C., and Helenius, A. (2016). Cargo Capture and Bulk Flow in the Early Secretory Pathway. Annu. Rev. Cell Dev. Biol. *32*, 197–222.

Blumer, J.B., and Lanier, S.M. (2014). Activators of G protein signaling exhibit broad functionality and define a distinct core signaling triad. Mol. Pharmacol. *85*, 388–396.

Boncompain, G., Divoux, S., Gareil, N., de Forges, H., Lescure, A., Latreche, L., Mercanti, V., Jollivet, F., Raposo, G., and Perez, F. (2012). Synchronization of secretory protein traffic in populations of cells. Nat. Methods *9*, 493–498.

Bonfanti, L., Mironov, A.A., Jr., Martínez-Menárguez, J.A., Martella, O., Fusella, A., Baldassarre, M., Buccione, R., Geuze, H.J., Mironov, A.A., and Luini, A. (1998). Procollagen traverses the Golgi stack without leaving the lumen of cisternae: evidence for cisternal maturation. Cell *95*, 993–1003.

Cancino, J., Capalbo, A., Di Campli, A., Giannotta, M., Rizzo, R., Jung, J.E., Di Martino, R., Persico, M., Heinklein, P., Sallese, M., and Luini, A. (2014). Control systems of membrane transport at the interface between the endoplasmic reticulum and the Golgi. Dev. Cell *30*, 280–294.

Carr, D.W., Hausken, Z.E., Fraser, I.D., Stofko-Hahn, R.E., and Scott, J.D. (1992). Association of the type II cAMP-dependent protein kinase with a human thyroid RII-anchoring protein. Cloning and characterization of the RII-binding domain. J. Biol. Chem. *267*, 13376–13382.

Choi, Y.H., Park, S., Hockman, S., Zmuda-Trzebiatowska, E., Svennelid, F., Haluzik, M., Gavrilova, O., Ahmad, F., Pepin, L., Napolitano, M., et al. (2006). Alterations in regulation of energy homeostasis in cyclic nucleotide phosphodiesterase 3B-null mice. J. Clin. Invest. *116*, 3240–3251.

Choudhary, C., Olsen, J.V., Brandts, C., Cox, J., Reddy, P.N., Böhmer, F.D., Gerke, V., Schmidt-Arras, D.E., Berdel, W.E., Müller-Tidow, C., et al. (2009). Mislocalized activation of oncogenic RTKs switches downstream signaling outcomes. Mol. Cell *36*, 326–339.

Cooper, D.M. (2005). Compartmentalization of adenylate cyclase and cAMP signalling. Biochem. Soc. Trans. *33*, 1319–1322.

de Opakua, A.I., Parag-Sharma, K., DiGiacomo, V., Merino, N., Leyme, A., Marivin, A., Villate, M., Nguyen, L.T., de la Cruz-Morcillo, M.A., Blanco-Canosa, J.B., et al. (2017). Molecular mechanism of Gαi activation by non-GPCR proteins with a Gα-Binding and Activating motif. Nat. Commun. *8*, 15163.

Diviani, D., Soderling, J., and Scott, J.D. (2001). AKAP-Lbc anchors protein kinase A and nucleates Galpha 12-selective Rho-mediated stress fiber formation. J. Biol. Chem. *276*, 44247–44257.

Dolfi, S.C., Chan, L.L., Qiu, J., Tedeschi, P.M., Bertino, J.R., Hirshfield, K.M., Oltvai, Z.N., and Vazquez, A. (2013). The metabolic demands of cancer cells are coupled to their size and protein synthesis rates. Cancer Metab. *1*, 20.

Doyle, J.C., Francis, B.A., and Tannenbaum, A. (1992). Feedback Control Theory (Macmillan).

Duan, B., Davis, R., Sadat, E.L., Collins, J., Sternweis, P.C., Yuan, D., and Jiang, L.I. (2010). Distinct roles of adenylyl cyclase VII in regulating the immune responses in mice. J. Immunol. *185*, 335–344.

Fanelli, F., and Dell'orco, D. (2008). Dark and photoactivated rhodopsin share common binding modes to transducin. FEBS Lett. *582*, 991–996.

Farhan, H., Weiss, M., Tani, K., Kaufman, R.J., and Hauri, H.P. (2008). Adaptation of endoplasmic reticulum exit sites to acute and chronic increases in cargo load. EMBO J. *27*, 2043–2054.

Farhan, H., Wendeler, M.W., Mitrovic, S., Fava, E., Silberberg, Y., Sharan, R., Zerial, M., and Hauri, H.P. (2010). MAPK signaling to the early secretory pathway revealed by kinase/phosphatase functional screening. J. Cell Biol. *189*, 997–1011.

Forster, R., Weiss, M., Zimmermann, T., Reynaud, E.G., Verissimo, F., Stephens, D.J., and Pepperkok, R. (2006). Secretory cargo regulates the turnover of COPII subunits at single ER exit sites. Curr. Biol. *16*, 173–179.

Giannotta, M., Ruggiero, C., Grossi, M., Cancino, J., Capitani, M., Pulvirenti, T., Consoli, G.M., Geraci, C., Fanelli, F., Luini, A., and Sallese, M. (2012). The KDEL receptor couples to Gαq/11 to activate Src kinases and regulate transport through the Golgi. EMBO J. *31*, 2869–2881.

Gordon, D.E., Bond, L.M., Sahlender, D.A., and Peden, A.A. (2010). A targeted siRNA screen to identify SNAREs required for constitutive secretion in mammalian cells. Traffic *11*, 1191–1204.

Gorur, A., Yuan, L., Kenny, S.J., Baba, S., Xu, K., and Schekman, R. (2017). COPII-coated membranes function as transport carriers of intracellular procollagen I. J. Cell Biol. *216*, 1745–1759.

Jiang, L.I., Collins, J., Davis, R., Fraser, I.D., and Sternweis, P.C. (2008). Regulation of cAMP responses by the G12/13 pathway converges on adenylyl cyclase VII. J. Biol. Chem. *283*, 23429–23439.

Koide, H., Holmbeck, K., Lui, J.C., Guo, X.C., Driggers, P., Chu, T., Tatsuno, I., Quaglieri, C., Kino, T., Baron, J., et al. (2015). Mice Deficient in AKAP13 (BRX) Are Osteoporotic and Have Impaired Osteogenesis. J. Bone Miner. Res. *30*, 1887–1895.

Kreutz, B., Yau, D.M., Nance, M.R., Tanabe, S., Tesmer, J.J., and Kozasa, T. (2006). A new approach to producing functional G alpha subunits yields the activated and deactivated structures of G alpha(12/13) proteins. Biochemistry *45*, 167–174.

Lee, T.H., and Linstedt, A.D. (2000). Potential role for protein kinases in regulation of bidirectional endoplasmic reticulum-to-Golgi transport revealed by protein kinase inhibitor H89. Mol. Biol. Cell *11*, 2577–2590.

Lee, S.J., Lee, W.H., Lee, C.H., and Kim, S.G. (2008). Regulation of thymus-dependent and thymus-independent production of immunoglobulin G subclasses by Galpha12 and Galpha13. J. Mol. Signal. *3*, 12.

Ma, W., Goldberg, E., and Goldberg, J. (2017). ER retention is imposed by COPII protein sorting and attenuated by 4-phenylbutyrate. eLife *6*, e26624.

Mancias, J.D., and Goldberg, J. (2008). Structural basis of cargo membrane protein discrimination by the human COPII coat machinery. EMBO J. *27*, 2918–2928.

Manni, S., Mauban, J.H., Ward, C.W., and Bond, M. (2008). Phosphorylation of the cAMP-dependent protein kinase (PKA) regulatory subunit modulates PKA-AKAP interaction, substrate phosphorylation, and calcium signaling in cardiac cells. J. Biol. Chem. *283*, 24145–24154.

Manzano-Lopez, J., Perez-Linero, A.M., Aguilera-Romero, A., Martin, M.E., Okano, T., Silva, D.V., Seeberger, P.H., Riezman, H., Funato, K., Goder, V., et al. (2015). COPII coat composition is actively regulated by luminal cargo maturation. Curr. Biol. *25*, 152–162.

Miller, E.A., Beilharz, T.H., Malkus, P.N., Lee, M.C., Hamamoto, S., Orci, L., and Schekman, R. (2003). Multiple cargo binding sites on the COPII subunit Sec24p ensure capture of diverse membrane proteins into transport vesicles. Cell *114*, 497–509.

Mironov, A.A., Mironov, A.A., Jr., Beznoussenko, G.V., Trucco, A., Lupetti, P., Smith, J.D., Geerts, W.J., Koster, A.J., Burger, K.N., Martone, M.E., et al. (2003). ER-to-Golgi carriers arise through direct en bloc protrusion and multistage maturation of specialized ER exit domains. Dev. Cell *5*, 583–594.

Nehls, S., Snapp, E.L., Cole, N.B., Zaal, K.J., Kenworthy, A.K., Roberts, T.H., Ellenberg, J., Presley, J.F., Siggia, E., and Lippincott-Schwartz, J. (2000). Dynamics and retention of misfolded proteins in native ER membranes. Nat. Cell Biol. *2*, 288–295.

Nishimura, N., and Balch, W.E. (1997). A di-acidic signal required for selective export from the endoplasmic reticulum. Science *277*, 556–558.

Nishimura, N., Bannykh, S., Slabough, S., Matteson, J., Altschuler, Y., Hahn, K., and Balch, W.E. (1999). A di-acidic (DXE) code directs concentration of cargo during export from the endoplasmic reticulum. J. Biol. Chem. *274*, 15937–15946.

Omori, K., and Kotera, J. (2007). Overview of PDEs and their regulation. Circ. Res. *100*, 309–327.

Pagant, S., Wu, A., Edwards, S., Diehl, F., and Miller, E.A. (2015). Sec24 is a coincidence detector that simultaneously binds two signals to drive ER export. Curr. Biol. *25*, 403–412.

Pahl, H.L., and Baeuerle, P.A. (1997). The ER-overload response: activation of NF-kappa B. Trends Biochem. Sci. *22*, 63–67.

Pakos-Zebrucka, K., Koryga, I., Mnich, K., Ljujic, M., Samali, A., and Gorman, A.M. (2016). The integrated stress response. EMBO Rep. *17*, 1374–1395.

Pierce, B.G., Hourai, Y., and Weng, Z. (2011). Accelerating protein docking in ZDOCK using an advanced 3D convolution library. PLoS ONE *6*, e24657.

Presley, J.F., Cole, N.B., Schroer, T.A., Hirschberg, K., Zaal, K.J., and Lippincott-Schwartz, J. (1997). ER-to-Golgi transport visualized in living cells. Nature *389*, 81–85.

Pulvirenti, T., Giannotta, M., Capestrano, M., Capitani, M., Pisanu, A., Polishchuk, R.S., San Pietro, E., Beznoussenko, G.V., Mironov, A.A., Turacchio, G., et al. (2008). A traffic-activated Golgi-based signalling circuit coordinates the secretory pathway. Nat. Cell Biol. *10*, 912–922.

Ron, D., and Harding, H.P. (2012). Protein-folding homeostasis in the endoplasmic reticulum and nutritional regulation. Cold Spring Harb. Perspect. Biol. *4*, a013177.

Rusu, L., Andreeva, A., Visintine, D.J., Kim, K., Vogel, S.M., Stojanovic-Terpo, A., Chernaya, O., Liu, G., Bakhshi, F.R., Haberichter, S.L., et al. (2014). G protein-dependent basal and evoked endothelial cell vWF secretion. Blood *123*, 442–450.

Saito, K., Chen, M., Bard, F., Chen, S., Zhou, H., Woodley, D., Polischuk, R., Schekman, R., and Malhotra, V. (2009). TANGO1 facilitates cargo loading at endoplasmic reticulum exit sites. Cell *136*, 891–902.

Sali, A., and Blundell, T.L. (1993). Comparative protein modelling by satisfaction of spatial restraints. J. Mol. Biol. *234*, 779–815.

Scott, J.D., Dessauer, C.W., and Taskén, K. (2013). Creating order from chaos: cellular regulation by kinase anchoring. Annu. Rev. Pharmacol. Toxicol. *53*, 187–210.

Shafiee-Nick, R., Afshari, A.R., Mousavi, S.H., Rafighdoust, A., Askari, V.R., Mollazadeh, H., Fanoudi, S., Mohtashami, E., Rahimi, V.B., Mohebbi, M., et al. (2017). A comprehensive review on the potential therapeutic benefits of phosphodiesterase inhibitors on cardiovascular diseases. Biomed. Pharmacother. *94*, 541–556.

Simpson, J.C., Cetin, C., Erfle, H., Joggerst, B., Liebel, U., Ellenberg, J., and Pepperkok, R. (2007). An RNAi screening platform to identify secretion machinery in mammalian cells. J. Biotechnol. *129*, 352–365.

Taylor, S.S., Kim, C., Cheng, C.Y., Brown, S.H., Wu, J., and Kannan, N. (2008). Signaling through cAMP and cAMP-dependent protein kinase: diverse strategies for drug design. Biochim. Biophys. Acta *1784*, 16–26.

van Anken, E., Romijn, E.P., Maggioni, C., Mezghrani, A., Sitia, R., Braakman, I., and Heck, A.J. (2003). Sequential waves of functionally related proteins are expressed when B cells prepare for antibody secretion. Immunity *18*, 243–253.

Walter, P., and Ron, D. (2011). The unfolded protein response: from stress pathway to homeostatic regulation. Science *334*, 1081–1086.

Wettschureck, N., and Offermanns, S. (2005). Mammalian G proteins and their cell type specific functions. Physiol. Rev. *85*, 1159–1204.

Wong, W., and Scott, J.D. (2004). AKAP signalling complexes: focal points in space and time. Nat. Rev. Mol. Cell Biol. *5*, 959–970.

Yamaguchi, Y., Katoh, H., and Negishi, M. (2003). N-terminal short sequences of alpha subunits of the G12 family determine selective coupling to receptors. J. Biol. Chem. *278*, 14936–14939.

STAR★METHODS

KEY RESOURCES TABLE

REAGENT or RESOURCE	SOURCE	IDENTIFIER
Antibodies		
Polyclonal Rabbit Phospho-(Ser/Thr) PKA Substrate	Cell Signaling Technology	Cat #9621; RRID:AB_330304
Monoclonal Mouse GAPDH	Santa Cruz Biotechnology	Clone 6C5 Cat #sc-32233; RRID: AB_627679
Monoclonal Rabbit phospho eIF2α (Anti-eIF2S1phospho S51)	Abcam	Clone E90 Cat #ab32157; RRID: AB_732117
Polyclonal Rabbit eIF2α	Cell Signaling Technology	Cat #9722; RRID:AB_2230924
Polyclonal Rabbit Phospho-p44/42 MAPK (Erk1 or Erk2) (Thr202/Tyr204)	Cell Signaling Technology	Cat #9101; RRID:AB_331646
Polyclonal Rabbit ERK-1 Antibody (also detects ERK2)	Santa Cruz Biotechnology	K-23 Cat #sc-94; RRID:AB_2140110
Polyclonal Rabbit Phospho-Akt (Ser473)	Cell Signaling Technology	Cat #9271; RRID:AB_329825
Polyclonal Rabbit VSV-G	Bethyl Laboratories Inc.	Cat #A190-131A; RRID:AB_155862
Monoclonal Mouse VSV-G	Sigma	SAB4200695
Monoclonal Mouse Sec31A	BD Biosciences	Clone 32 Cat #612351; RRID: AB_399717
Monoclonal Mouse Collagen, Type I pro-peptide (PC-I total)	Developmental Studies Hybridoma Bank	Clone SP1.D8; RRID:AB_528438
Polyclonal Rabbit GRASP55	Novus Biologicals	Cat #NBP1-89747; RRID:AB_11024556
Polyclonal Rabbit PKA IIα reg (PKA-RIIa)	Santa Cruz Biotechnology	C-20 Cat #sc-908; RRID:AB_632214
Monoclonal Mouse Myc-Tag	Cell Signaling Technology	Clone 9B11 Cat #2276; RRID:AB_331783
Polyclonal Rabbit Myc-Tag	Cell Signaling Technology	Cat #2272S; RRID:AB_10692100
Polyclonal Rabbit Gα12	Santa Cruz Biotechnology	S-20 Cat #sc-409; RRID:AB_2263416
Monoclonal Mouse Gα12	Santa Cruz Biotechnology	Clone E-12 Cat #sc-515445
Polyclonal Goat Sec24A	Santa Cruz Biotechnology	Cat #sc-169279; RRID:AB_10841885
Polyclonal Rabbit Sec24A	Cell Signaling Technology	Cat #9678; RRID:AB_10949103
Monoclonal Mouse HA-Tag	Biolegend/Covance	Clone 16B12 Cat #MMS-101P; RRID: AB_10063630
Monoclonal Rabbit HA-Tag	Cell Signaling Technology	Clone C29F4; Cat #3724
Polyclonal Sheep anti-human TGN46	BioRad/AbD-Serotec	Cat #AHP500G; RRID:AB_323104
Polyclonal Rabbit AKAP-Lbc/AKAP13	Bethyl Laboratories Inc.	Cat #A301-404A; RRID:AB_960932
Polyclonal Rabbit Sec23A	Cell Signaling Technology	Cat #8162; RRID:AB_10859891
Monoclonal Mouse anti-β Actin	Sigma	Clone AC-74 Cat #A2228; RRID: AB_476697
Monoclonal Mouse Gα13	EMD Millipore/Calbiochem	Clone 6F6-B5 Cat #ST1629; RRID: AB_10694747
Monoclonal Mouse Calnexin	Santa Cruz Biotechnology	Clone AF18 Cat #sc-23954; RRID: AB_626783
Monoclonal Mouse PDI	Novus Biologicals	Clone RL90 Cat #NB300-517; RRID: AB_2156591
Polyclonal Rabbit GRP78 or BiP	Novus Biologicals	Cat #NBP1-06274; RRID:AB_1555284
Polyclonal Rabbit Phospho-PKR (Thr446)	Thermo Scientific/Invitrogen	Cat #PA5-37704; RRID:AB_2554312
Polyclonal Rabbit PKR	Santa Cruz Biotechnology	Clone K-17 Cat #sc-707; RRID:AB_632244
Monoclonal Mouse PERK	Santa Cruz Biotechnology	Clone B-5 Cat #sc-377400
Polyclonal Rabbit MIA3/TANGO-1	Santa Cruz Biotechnology	Clone H-156 Cat #sc-366098

(*Continued on next page*)

Continued

REAGENT or RESOURCE	SOURCE	IDENTIFIER
Monoclonal Mouse antibody against the helical portion of Collagen-I [hCL(I)] (PC-I folded)	Kind gift from Rossella Venditti and Antonella de Matteis, TIGEM, Pozzuoli	Clone I-8H5; RRID:AB_10675468
Polyclonal Rabbit Sec13	Bethyl Laboratories Inc.	Cat #A303-980A; RRID:AB_2620329
Monoclonal Rabbit Anti-PKA R2 (phospho S96)	Abcam	Clone E151 Cat #ab32390; RRID: AB_779040
Monoclonal Mouse Hsc70	Enzo Life Sciences	Clone 13D3 Cat # ALX-804-067-R050; RRID:AB_2051627
Monoclonal Mouse GFP	Abcam	Cat #ab6556; RRID:AB_305564
Polyclonal Rabbit Sar1A	EMD Millipore	Cat #07-692; RRID:AB_417400
Polyclonal Rabbit PKAα Catalytic subunit	Santa Cruz Biotechnology	Clone C-20 Cat #sc-903; RRID: AB_2268772
Mouse Monoclonal FLAG-tag	Sigma	Clone M2 Cat #P2983; RRID:AB_439685
Mouse Monoclonal AKAP2/AKAP-KL	BD Biosciences	Clone 41 Cat #611134; RRID:AB_398445
Polyclonal Rabbit PDE3B	Sigma/Atlas Antibodies	Cat #HPA056111; RRID:AB_2683041
Monoclonal Goat Sec24B	Santa Cruz Biotechnology	Clone I-16 Cat #sc-160785; RRID: AB_2186120
Polyclonal Rabbit phospho-p38 MAPK (Thr180/Tyr182)	Cell Signaling Technology	Cat #9211; RRID:AB_331641
Polyclonal Rabbit p38 MAPK	Cell Signaling Technology	Cat #9212; RRID:AB_330713
Monoclonal Rabbit phospho-CREB (Ser133)	Cell Signaling Technology	Clone 87G3; Cat #9198 RRID:AB_2561044
Monoclonal Rabbit CREB	Cell Signaling Technology	Clone 48H2; Cat #9197 RRID:AB_331277
Anti-mouse, donkey Alexa Fluor 488	ThermoFisher Scientific	Cat #A-21202; RRID:AB_141607
Anti-mouse, donkey Alexa Fluor 568	ThermoFisher Scientific	Cat #A10037; RRID:AB_2534013
Anti-mouse, goat Alexa Fluor 633	ThermoFisher Scientific	Cat #A-21052; RRID:AB_141459
Anti-rabbit, donkey Alexa Fluor 488	ThermoFisher Scientific	Cat #A-21206; RRID:AB_141708
Anti-rabbit, donkey Alexa Fluor 568	ThermoFisher Scientific	Cat #A10042; RRID:AB_2534017
Anti-rabbit, goat Alexa Fluor 633	ThermoFisher Scientific	Cat #A-21070; RRID:AB_2535731
Anti-sheep, donkey Alexa Fluor 633	ThermoFisher Scientific	Cat #A-21100; RRID:AB_2535754
Anti-goat, donkey Alexa Fluor 568	ThermoFisher Scientific	Cat #A-11057; RRID:AB_142581
Bacterial and Viral Strains		
Temperature sensitive strain of vesicular stomatitis virus (ts045-VSV)	Kind gift from Bruno Goud, Institut Curie, France	*N/A*
E.coli (DH5α)	Thermo Fisher Scientific	Cat #18265017
E.coli (BL-21-DE3)	Thermo Fisher Scientific	Cat #C600003
Chemicals, Peptides and Recombinant Proteins		
PD98059	Sigma	Cat #P215
PKI-1422	EMD Millipore/Calbiochem	Cat #476485
FPA-124	Tocris	Cat #2926
Paraformaldehyde 8%	Electron Microscopy Sciences	Cat #50-259-96
Glutaraldehyde 8%	Electron Microscopy Sciences	Cat #50-262-18
Methanol	JT Baker	Cat #9093
Cycloheximide	Sigma	Cat #01810
Ascorbic Acid	Sigma	Cat #A4544
8-Br-cAMP	Tocris	Cat #1140
Trequinsin hydrochloride (PDE3 inhibitor)	Sigma	Cat #T2057
Forskolin	Calbiochem	Cat #344270
InCELLect AKAP St-Ht31inhibitor peptide	Promega	Cat #V821A
Protein A Sepharose CL-4B	GE Healthcare Life Sciences	Cat #17-0780-01

(*Continued on next page*)

Continued

REAGENT or RESOURCE	SOURCE	IDENTIFIER
Anti-c-myc magnetic beads	ThermoFisher Scientific	Cat #88843
Anti-HA magnetic beads	ThermoFisher Scientific	Cat #88836
Guanosine 5′-[γ-thio]triphosphate tetralithium salt (GTP-γS)	Sigma	Cat #G8634
Guanosine 5′-triphosphate sodium salt hydrate (GTP)	Sigma	Cat #G8877
Guanosine 5′-diphosphate sodium salt (GDP)	Sigma	Cat #G7127
GTPγS, [35S]	Perkin Elmer	Cat #NEG030H001MC
c-Myc Peptide	Sigma	Cat #M2435
HA Peptide	Sigma	Cat #I2149
SYPRO® Ruby Protein Gel Stain	ThermoFisher Scientific	Cat #S12000
Recombinant Sec24B-FLAG/Myc, transcript variant 2	Origene	Cat #TP319074
Tunicamycin from Streptomyces sp	Sigma	Cat #T7765
Thapsigargin	Sigma	Cat #T9033
VSVG cytosolic tail DIE peptide – RRRRRRRRGQIYTDIEMNR-CONH2	This study	*N/A*
VSVG cytosolic tail mutant AAA peptide – RRRRRRRRGQIYTAAAMNR-CONH2	This study	*N/A*
Isoprenaline hydrochloride	Sigma	Cat #I5627
Recombinant TPR-PP5, GST tagged	Produced inhouse; construct was a kind gift from Philip Wedegaertner and Manabu Negishi (Yamaguchi et al., 2003)	*N/A*
EasyTag EXPRESS35S Protein Labeling Mix, [35S]	Perkin Elmer	Cat #NEG772014MC
Brefeldin A	Sigma	Cat #B7651
DD solubilizer	Clontech	Cat #635054
Biotin	Pierce	Cat #29129
Protein A gold 15nm	Cell Microscopy Core, UMC Utrecht	*N/A*
Protein A gold 10nm	Cell Microscopy Core, UMC Utrecht	*N/A*
Lipofectamine 2000	ThermoFisher Scientific	Cat #11668027
Lipofecatime LTX with PLUS	ThermoFisher Scientific	Cat #15338100
Oligofectamine	ThermoFisher Scientific	Cat #12252011
TransIT-LT1	Mirus	Cat #MIR 2305
DMEM	GIBCO/ ThermoFisher Scientific	Cat #41965
RPMI 1640	GIBCO/ ThermoFisher Scientific	Cat #21875
FBS	GIBCO/ ThermoFisher Scientific	Cat #10437036
DMEM w/o cysteine and methionine	GIBCO/ ThermoFisher Scientific	Cat #21013
Critical Commercial Assays		
Endo-H	NEB	Cat #P0702S
RNA easy mini	QIAGEN	Cat #74106
QuantiTect Reverse Transcription Kit Print	QIAGEN	Cat #205311
SYBR Green PCR Master Mix	ThermoFisher Scientific	Cat #4309155
Kinexus Antibody Microarray	Kinexus	Cat #KAM-880
Experimental Models: Cell Lines		
HeLa-M	ATCC	RRID:CVCL_R965
Primary Human Fibroblasts	This study; Telethon Biobank ((http://biobanknetwork.telethon.it/)	*N/A*
Immortalized human fibroblasts-BJ-5ta	ATCC	RRID:CVCL_6573

(*Continued on next page*)

Continued

REAGENT or RESOURCE	SOURCE	IDENTIFIER
HeLa stably transfected with hGH-FM-GFP	Gift from Andrew Peden (Gordon et al., 2010)	*N/A*
Wild type MEFs	Gift from SG Kim	*N/A*
Gna12 knockout MEFs	Gift from SG Kim	*N/A*
Recombinant DNA		
ts045-VSVG-GFP (VSVG-DXE-GFP)	(Presley et al., 1997)	Addgene, Cat #11912
ADCY7-myc	Origene	Cat #RC214351
ts045-VSVG-AIA-GFP (VSVG-AXA-GFP)	Kind gift from William E Balch, Scripps Institute, La Jolla	*N/A*
ts045-VSVG-mcherry	Kind gift from Jorge Cancino, Chile	*N/A*
TPR-PP5-GST	Kind gift from Manabu Negishi and provided to us by Philip Wedegaertner, Thomas Jefferson University	*N/A*
TPR-PP5-HA	This study; Subcloned into pcDNA3.1-3xHA from TPR-PP5-GST	*N/A*
Gα12WT-myc	Kind gift from Thomas Meigs, UNC	*N/A*
Gα12G228A-myc (GDP-Gα12)	Kind gift from Thomas Meigs, UNC	*N/A*
Gα12Q229L-myc (GTP- Gα12)	Kind gift from Thomas Meigs, UNC	*N/A*
Sec13-GFP	Kind gift from Benjamin Glick, U Chicago and Antonella de Matteis, TIGEM	*N/A*
Sec24A-HA	Kind gift from Randy Schekman, Berkely	*N/A*
Sec24B-HA	Kind gift from Randy Schekman, Berkely	*N/A*
Sec24C-HA	Kind gift from Randy Schekman, Berkely	*N/A*
Sec24D-HA	Kind gift from Randy Schekman, Berkely	*N/A*
PDE3B-myc	Origene	Cat #RC219619
Sec24A-ΔTHEG4-HA	This study	*N/A*
Sec24A-ΔZF-HA	This study	*N/A*
Sec24A-ΔvWFA-HA	This study	*N/A*
Sec24A-Δβ/S-HA	This study	*N/A*
Sec24A-ΔHelical-HA	This study	*N/A*
Sec24A-ΔADF Gelosin-HA	This study	*N/A*
Sec24A β/S domain-FLAG	This study	*N/A*
Sialyl transferase-RFP	Kind gift from Seetharaman Parashuraman, IBP, Naples	*N/A*
Ii-Str_SBP-mCherry-E-Cadherin	(Boncompain et al., 2012)	Addgene, Cat #65289
Ii-Str_SBP-EGFP-E-Cadherin	(Boncompain et al., 2012)	Addgene, Cat #65288
CFP-Epac-(dDEP)-YFP (EPAC)	Kind gift from Manuela Zaccolo, UK	*N/A*
PKAcat- YFP/PKAreg-CFP	Kind gift from Manuela Zaccolo, UK	*N/A*
siRNA resistant full length AKAP-Lbc-FLAG	Kind gift from Dario Diviani, Switzerland	*N/A*
siRNA resistant AKAP-Lbc-FLAG PKA binding mutant (A1251P/I1260P)	Backbone plasmid was a kind gift from Dario Diviani, Switzerland. siRNA resistance was performed for this study	*N/A*
Software and Algorithms		
ImageJ	NIH	https://imagej.nih.gov/ij/
MetaMorph	Molecular Devices	https://www.moleculardevices.com/products/cellular-imaging-systems/acquisition-and-analysis-software/metamorph-microscopy
Prism	Graphpad	https://www.graphpad.com/scientific-software/prism/

(*Continued on next page*)

Continued

REAGENT or RESOURCE	SOURCE	IDENTIFIER
Zen Lite	Carl Zeiss	https://www.zeiss.com/microscopy/int/products/microscope-software/zen-lite.html
Adobe Illustrator	Adobe	https://www.adobe.com/products/illustrator/free-trial-download.htm
Adobe Photoshop	Adobe	https://www.adobe.com/products/photoshop.html
Soft Imaging service (Electron microscope)	Olympus	https://www.olympus-sis.com/corp/2256.htm
iTEM	EMSIS GmbH	https://www.emsis.eu/products/software/item/
Oligonucleotides		
see Table S2		

CONTACT FOR REAGENT AND RESOURCE SHARING

Further information and requests for resources and reagents should be directed to and will be fulfilled by Lead Contact, Alberto Luini (a.luini@ibp.cnr.it).

EXPERIMENTAL MODEL AND SUBJECT DETAILS

Cell lines

HeLa-M (human cervical cancer cells, female origin) were obtained from the ATCC and grown in RPMI-1640 supplemented with 10% FCS. Primary Human Fibroblasts (Normal Control, male origin) were obtained from the Telethon Biobank and grown in DMEM supplemented with 1% sodium pyruvate and 20% FCS. BJ-5ta (human immortalized fibroblasts, male origin) were obtained from the ATCC and grown in DMEM: Nutrient Mixture F-12 (DMEM/F-12) supplemented with 10% FCS. HeLa-M cells stably transfected with hGH-FM-GFP (female origin) were a kind gift from A Peden (Gordon et al., 2010) and grown in DMEM supplemented with 10% FCS. For experiments with the SBP-FP-E-Cadherin (RUSH) constructs, HeLa-M cells were grown in DMEM supplemented with 10% FCS without biotin. Wild-type and Gα12 knockout mouse embryonic fibroblasts were kind gifts from SG Kim and grown in DMEM supplemented with 1% sodium pyruvate and 10% FCS. All media were supplemented with penicillin/streptomycin and L-glutamine. The cell lines have not been authenticated.

METHOD DETAILS

Transfection

HeLa-M cells were transfected with plasmid vectors using the TransIT-LT1 or Lipofectamine LTX reagents. Only cells expressing moderate levels of the respective plasmids were chosen for IF analyses. siRNA treatments were carried out using a pool of siRNAs and Lipofectamine 2000 for HeLa-M cells or Oligofectamine for primary human fibroblasts. Expression or knockdown efficiencies (> 85%) were checked after every experiment either by indirect immunofluorescence or immunoblotting. Each individual siRNA in the pool was also tested for knockdown and in transport assays with similar results. A list of siRNA sequences used in this study can be found in Table S2.

Cargo folding and transport pulses

Five synchronizable secretory cargos were used in this study – three temperature sensitive (ts) cargos ts045-VSVG (VSVG), ts045-VSVG-AXA-GFP (VSVG-AXA) and Procollagen-I (PC-I) and two molecular trap cargos SBP-FP-E-Cadherin and hGH-FM-GFP. VSVG viral infection was performed at 32°C for 1 h in FCS-free DMEM-HEPES medium. Cells then were washed 3 times with PBS and kept for 3 h at 40°C in DMEM-HEPES supplemented with 10% FCS to accumulate unfolded VSVG in the ER. For ts045-VSVG-GFP and ts045-VSVG-AXA-GFP transfections, cells were incubated with respective plasmids for 16 h at 40°C in an incubator with 5%CO_2. A folding pulse of VSVG or VSVG-AXA was induced by shifting the cells to 32°C for 4 min. An ER to Golgi transport pulse was induced by shifting cells to 32°C for 16 min or later time points as indicated (Mironov et al., 2003; Nishimura and Balch, 1997). Human fibroblast cultures or MEFs were washed 3 times with PBS and kept for 3h at 40°C in DMEM-HEPES supplemented with 1% FCS without

ascorbic acid. A folding (4min) or traffic pulse (8min or 16min) of PC-I was induced by shifting cells to 32°C in the presence of 100 μg/mL ascorbic acid (Mironov et al., 2003). Molecular trap cargo construct SBP-FP-E-Cahderin was transfected into HeLa cells cultured in DMEM supplemented with 10% FCS without biotin at 37°C. A short folding or longer traffic pulse was induced by treating cells with biotin (40 μg/mL) for the indicated times (Boncompain et al., 2012). Similarly, synchronous hGH-FM-GFP release from the ER of HeLa cells stably transfected with the cargo was performed by adding DD solubilizer (2μM) to the cells for the times indicated in each figure (Gordon et al., 2010). Cycloheximide (CHX; 50 μg/mL) was added 30 min before all folding and traffic pulse experiments to ensure that a majority of the secretory cargo monitored and the response it generates in the cell was specific. We however note that proteins that aid in the ER export process, such as adaptors or SNAREs (machinery cargo) may interact with the COPII export machinery just like secreted cargo but are recycled back to the ER after use and are long-lived, and hence not affected by CHX. However, they are much less abundant than the secreted cargo, especially when the latter is abundantly expressed, as in our case, or in 'professional' secretory cells.

Targeted phosphoproteomics by antibody microarray and analysis

HeLa cells infected with VSVG virus or Primary Human Fibroblasts with endogenous PC-I were subjected to folding block (40°C 3 h, see above) or a folding pulse (32°C 2 or 4 min). Cells were lysed in lysis buffer (50 mM HEPES, pH 7.4, 100 mM NaCl, 0.5% NP-40, 30 mM NaF, 2 mM Na3O4V, 60 mM β-glycerophosphate, 5 mM EDTA, 5 mM EGTA, and the protease inhibitor cocktail from Roche) and the protein concentrations were quantified using BCA kits (Pierce). Protein samples were frozen at −80°C before being subjected to an antibody microarray (KAM-880 array) and data analysis, which was performed at Kinexus (System proteomic company, Vancouver, Canada). The array monitors changes in the expression levels and phosphorylation states of signaling proteins which includes 518 pan-specific antibodies (for protein expression) and 359 phospho- site-specific antibodies (for phosphorylation). The resultant changes are expressed as percentages of change with respect to the control (CFC) and as Z-factors. Changes $\geq$ 50% CFC and Z ratio $\geq$ +1.00 (hyper phosphorylation) or $\leq$ −1.00 (dephosphorylation) were considered as real significant changes. Only proteins whose phosphorylation status differed after the folding pulse were considered, analyzed by bioinformatic tools such as Ingenuity Pathway Analysis, DAVID-KEGG pathway, STRING and PhosphoSite plus and built into signaling pathway maps or networks manually using Adobe Illustrator (Adobe systems).

Inhibitor and peptide treatments

All inhibitors and cell permeant peptides were tested for purity and efficacy before use. In most experiments, cells were pretreated with them for 1 h unless otherwise specified. The effective concentration of PKI-1422 in reducing basal and forskolin stimulated PKA activity was determined to be 100 μM by immunoblotting for phosphorylated PKA substrates (data not shown). The small molecule inhibitors of ERK1 or ERK2 (PD98059/25μM) and Akt (FPA-124/10μM) were used at concentrations deemed effective in blocking kinase activity in cells.

Generation of siRNA resistant constructs

AKAP-Lbc-FLAG-ΔPKA [AKAP-Lbc-FLAG A1251P/I1260P (Diviani et al., 2001)] siRNA resistant construct was generated by site-directed mutagenesis. The oligonucleotide primers used for the mutagenesis reaction were: 5′-GCAAAGTGGCAAGTTAT GAAAAGAAAGTAAGATTAAACGAAATCTATACAAAGACAGATAGCAAGTCAATCATGAGG-3′ and 5′-CCTCATGATTGACTTGCTAT CTGTCTTTGTATAGATTTCGTTTAATCTTACTTTCTTTTCATAACTTGCCACTTTGC-3′. PCR conditions for mutagenesis reaction were as follows: a single denaturation step (95°C, 5 min) was performed and followed by 20 cycles of denaturation (95°C, 1 min), annealing (60°C, 1 min) and elongation (68°C, 30 min). Then a final elongation step of 10 min at 72°C was performed. The PCR reaction was carried out in a 50 μl final volume including the following components: 50 ng of DNA template, 500 μM of each dNTPs, 1.5x PfuTurbo Cx Hotstart DNA Polymerase buffer, 0.2 μM of each primer and 5 U of PfuTurbo Cx Hotstart DNA Polymerase.

Following completion of mutagenesis reactions, parental plasmid DNA was digested by DpnI treatment (20 U/mutagenesis reaction) for 1 h at 37°C. Then DNA was precipitated, resuspended in sterile water and transformed into chemical competent *E. coli* TOP-10 cells.

Confocal microscopy

Images were acquired using a Zeiss LSM710 using a 40x or 63 × oil-immersion objective (1.4 NA) using identical setting for each channel throughout single experiments.

Details are mentioned below.

Indirect immunofluorescence: indirect immunofluorescence (IF) was performed as follows: cells grown on coverslips were washed in phosphate-buffered saline (PBS) and fixed in freshly prepared PBS supplemented with 4% paraformaldehyde (Electron Microscopy Sciences, Hatfield, USA) for 30 min at room temperature (RT) for most experiments. Cells were permeabilized and blocked in blocking buffer (0.05% saponin in 0.5% BSA) for 30 min at room temperature. Primary antibodies were incubated for 1h at RT or overnight at 4°C in blocking buffer. Cells were subsequently labeled with appropriate Alexa 488/568/633-tagged fluorescent-conjugated secondary antibodies. For IF experiments including the staining for Sec24A, cells were grown on

coverslips, washed with PBS and fixed with ice cold 100% methanol for 5 min at −20°C. Cells were then blocked with 5% (w/v) BSA in PBS at RT. Primary antibodies were incubated for 1h at RT in 5% BSA and subsequently labeled with appropriate Alexa 488/568/633-tagged fluorescent-conjugated secondary antibodies.

Image processing: for Figure presentation only, the images were channel-separated, with each channel shown as color or grayscale image after correcting for contrast using Image-J (NIH) or Adobe Photoshop CS3 (Adobe Systems). In some cases, the contrast was inverted, and the levels adjusted to facilitate the observation of dim structures.

Live Cell Imaging

VSVG-GFP exit in control and PKI-1422 treated cells

HeLa-M cells transiently transfected with VSVG-GFP were grown in RPMI with 10% FCS at 40°C for 16h in glass-bottomed 35-mm dishes (MatTek Corporation, Ashland, MA 01721, USA). Cells were pretreated with vehicle (medium) or PKI-1422 (100 μM) for 1 h and cycloheximide (50 μg/mL) for 30 min at 40°C. Cells were then washed with PBS, and replenished with DMEM-HEPES containing inhibitors and cycloheximide and then mounted on a Zeiss LSM710 laser scanning microscope at 32°C, using a water-jacketed stage to regulate the temperature and running the Zen image acquisition software (Zeiss). Time lapse imaging was performed at 15 s intervals (488 laser for excitation; PMT: 510-550 nm; 1024 × 1024 pixels; frame average, 5). After acquisition, the video was processed and complied using Image-J. Representative frames were selected and processed for figure presentation.

Measuring formation of ER export carriers and bulk flow transport by monitoring VSVG-AXA-GFP exit in control and PDE3i treated cells

For these analyses, we used VSVG-AXA-GFP as a transport marker as it is reported to be unable to bind Sec24 and is exported to the Golgi slowly, apparently by bulk flow (Mancias and Goldberg, 2008; Nishimura and Balch, 1997; Nishimura et al., 1999). We thus carried out folding pulse experiments using VSVG-AXA-GFP. HeLa-M cells transiently co-transfected with VSVG-AXA-GFP and ST-RFP were grown in RPMI with 10% FCS at 40°C for 16h in glass-bottomed 35-mm dishes (MatTek Corporation, Ashland, MA 01721, USA). Cells were pretreated with vehicle (DMSO) or trequinsin hydrochloride (PDE3 inhibitor; 10 μM) for 1 h and cycloheximide (50 μg/mL) for 30 min at 40°C. Cells were then washed with PBS, and replenished with DMEM-HEPES containing inhibitors and cycloheximide and then mounted on a Zeiss LSM710 laser scanning microscope at 32°C, using a water-jacketed stage to regulate the temperature and running the Zen image acquisition software (Zeiss). Time lapse imaging was performed at 15 s intervals (488 laser for excitation of GFP; 568 laser for excitation of RFP; 1024 × 1024 pixels; frame average, 5). After acquisition, the video was processed and complied using Image-J. Representative frames were selected and line scan analysis was performed using MetaMorph software and processed for figure presentation.

FRET measurements

For folding pulse experiments, cells were placed in glass-bottomed 35-mm dishes (MatTek) and transfected with the VSVG-mcherry plasmid and the EPAC YFP/CFP FRET-pair for 16 h at 40°C, or the cells were co-microinjected and then kept for 3 h at 40°C in DMEM-HEPES. Before the experiment, the cells were incubated at 40°C with cycloheximide (100 μg/ml) for 30 min and then mounted on a Zeiss LSM710 laser scanning microscope at 40°C, using a water-jacketed stage to regulate the temperature and running the Zen image acquisition software (Zeiss). The temperature was kept at 40°C for 10 min before the start of the traffic pulse. Basal cAMP and PKA activities were recorded over 3-5 min at 40°C, and then for 10 min of traffic pulses at 10-30 s interval, using a 458-nm laser for excitation (CFP), and with simultaneous acquisition of CFP (480 nm) and YFP (514 nm) emissions (sensitized FRET). Sequential acquisition of VSVG-mcherry was carried out using 568-nm-wavelength lasers for excitation, with the 63 × oil-immersion objective. The CFP:YFP ratio was then quantitated (see below).

Electron microscopy

The samples were fixed and prepared using standard procedures, as previously described (Cancino et al., 2014).

Morphometric characterization of the early secretory pathway by Epon EM in control and PDE3i treatment conditions

Briefly, HeLa-M cells grown in 35mm plastic dishes were treated with DMSO or PDE3i (10 μM) for 1 h and cycloheximide (50 μg/mL) for the last 30 min of inhibitor incubation at 37°C. Cells were then fixed with 1% Glutaraldehyde (8% Aqueous Solution – Electron Microscopy Sciences) in HEPES 0.2M pH 7.3 at 4°C overnight. The fixative was replaced with 1% BSA in PBS and cells were carefully detached using a plastic cell scraper, collected into microfuge tubes and centrifuged to obtain the pellet. All samples were then washed three times in HEPES 0.2M pH 7.3 and post-fixed 30 min in 1% Osmium Tetroxide in the dark at 4°C in the same buffer. They were then washed three times in distilled water and post-fixed 25 min in 1% Osmium Tetroxide and 1.5% Potassium Ferrocyanide in the dark at room temperature in HEPES 0.2M pH 7.3. After washing three times in distilled water, they were stained with 0.5% uranyl acetate over night at 4°C. The pellets were dehydrated in graded steps of ethanol (50%, 70%, 90%, 100%), 2 times with 100% of acetone and embedded into Epon. Section (60 nm thick) were cut on a Leica UC7 ultramicrotome and examined with a Fei Tecnai 12 BioTwin Spirit transmission electron microscope.

Cryo-immuno EM

HeLa cells transiently transfected with VSVG-GFP or co-transfected with VSVG-GFP and Sec24A-HA were kept for 16 h at 40°C and subjected to a traffic pulse for 16' at 32°C in the absence or presence of PKI-1422 (100 μM). The cells were fixed with 2% formaldehyde and 0.2% glutaraldehyde in PHEM buffer (0.1M) pelleted by centrifugation, embedded in 12% gelatin, cooled on ice, and cut into 1-mm^3 cubes at 4°C. The cubes were immersed in 2.3 M sucrose at 4°C overnight, and then frozen in liquid nitrogen. Fifty-nanometre sections were cutted with a diamond knife on a UC7 Leica cryo-ultramicrotome. The sections were picked up in a mix of 2% methyl cellulose and 2.3 M sucrose (1:1), as previously described (Pulvirenti et al., 2008), and collected on grids covered with Formvar-carbon supporting film (Electron Microscopy Sciences, PA, USA). The grids were first incubated with the rabbit anti-GFP and/or rabbit anti-HA polyclonal antibodies and then incubated with different sizes of Protein A gold (10 nm and 15 nm) to revealed antigen staining. After labeling, the sections were treated with 1% glutaraldehyde and embedded in methyl cellulose uranyl acetate for 10 min on ice. The excess of methyl cellulose uranyl acetate was removed and the sections were dried at room temperature before their analysis at 120 kV in a Philips Tecnai 12 Biotwin electron microscope (FEI, Einhoven, the Netherlands) using a VELETA digital camera.

SDS–PAGE and Immunoblotting

the cells were washed three times with PBS and collected immediately at 4°C in RIPA lysis buffer (1% Triton X-100, 20mM Tris-HCl, pH 8.0, 0.1% SDS, 0.05% sodium deoxycholate, 150mM NaCl, 10mM Na3VO4, 40mM β-glycerophosphate, 10mM NaF) and complete protease inhibitors (5 × ; Roche). Cell lysates were centrifuged at 10,000 rpm for 10 min at 4°C to eliminate detergent insoluble pellet. The supernatant was immediately processed for SDS–PAGE and immunoblotting with antibodies.

Immunoprecipitation

total lysates were prepared using IP lysis buffer (150 mM NaCl, 25mM Tris-HCl pH = 7.5, 1% Triton-X, 10mM Na3VO4, 40mM β-glycerophosphate, 10mM NaF and protease cocktail inhibitor from Roche). The protein concentrations were quantified and 1mg of protein was used for immunoprecipitation with antibodies conjugated to either Protein A Sepharose or magnetic dynabeads.

Endo-H sensitivity assay

Cells treated with siRNAs were subjected to a VSVG transport pulse at 32°C. Total lysates were then boiled with denaturation buffer at 100°C and allowed to cool. Samples were then incubated with Glycobuffer and Endo-H enzyme at 37°C for 1 h followed by SDS-PAGE and western blotting for VSVG and loading controls.

Immunopurification of Sec24A and Gα12

HeLa-M cells were transiently transfected with HA-tagged Sec24A or myc-tagged Gα12 in separate 10cm plates for 24 h at 37°C. Cells were lysed with IP lysis buffer (150 mM NaCl, 25mM Tris-HCl pH = 7.5, 1% Triton-X, 10mM Na3VO4, 40mM β-glycerophosphate, 10mM NaF and protease cocktail inhibitor from Roche) either under this condition or after infection with VSVG virus and traffic block at 40°C for 3 h. Both proteins were immunoprecipitated with protein A Sepharose beads conjugated with HA or myc antibodies. The beads were then subjected to extensive washes (= 10) with lysis buffer and the respective proteins were extracted by incubating the beads with HA or myc peptides (100 μg/mL) at 4°C for 30 min. The purity of the eluted proteins was determined with SDS-PAGE and SYPRO-RUBY staining and appeared to be ~80% with some contaminants that included the antibody heavy and light chains. 25% of total immuno-isolated Gα12-myc was detectable by SYPRO-RUBY, but 25% of total immuno-isolated Sec24A-HA was not. Nevertheless, both the immuno-purified proteins were detectable by western blotting (data not shown). Notably, endogenous Sec23A was not present in the eluate in complex with Sec24A-HA, but was present in the beads fraction. Similarly, endogenous Sec24A was not present in the eluate in complex with Gα12-myc but was present in the beads fraction.

In vitro *GDP to GTP exchange assay*

Approximately 1 μg of immunopurified Sec24A-HA and Gα12-myc alone or in combination were incubated in assay buffer (100mM NaCl, 10mM $MgCl_2$, 10mM HEPES, pH = 7.4, 1 μM GDP, 100nM GTPγ-S) in the presence or absence of R8-DIE or the R8-AAA VSVG tail peptides (1 μM) for 30 min at 30°C. The reaction was terminated by addition of ice cold assay buffer without GDP/GTP-γS nucleotides. Recombinant GST tagged TPR-PP5 coupled to glutathione agarose beads was then added to all tubes and the degree of Gα12 activation under the various conditions was assessed by a GST pull down assay (Yamaguchi et al., 2003).

Radioactive GTP-γS35 incorporation assay:

The [^{35}S]GTPγS-binding assay follows a modified protocol previously described by Gianotta et al. (Giannotta et al., 2012). To detect [^{35}S]GTPγS binding to Gα12, immuno-purified Sec24A-HA and Gα12-myc proteins from HeLa cells were resuspended in 50 μL assay buffer (100mM NaCl, 10mM $MgCl_2$, and 10mM HEPES, pH 7.4) containing 2nM [^{35}S]GTPγS (1000 Ci/mmol) (Perkin-Elmer, USA), 2 μM GDP, without or with R8-AAA and R8-DIE peptides (2 μM) and then incubated at 30°C for 30 min. Gα12 was immunoprecipitated using myc antibody coupled to magnetic beads and the radioactivity was determined via scintillation counter.

Steady state traffic assays

For assays monitoring PC-I in primary human fibroblasts, cells transfected with siRNAs for 48 h were cultured at 37°C in DMEM supplemented with 20% FCS. In the last 24 h, the medium was removed, cells were washed extensively with DMEM supplemented with 1% FCS and incubated for 24 h in the same medium with 2 μg/mL ascorbic acid to promote PC-I synthesis, folding and secretion. The

medium was collected and the proteins were isolated with TCA and acetone washes (supernatant fraction). The pellet fraction was extracted with RIPA lysis buffer.

For assays monitoring PC-I in MEFs, cells were cultured at 37°C in DMEM supplemented with 10%FCS and sodium pyruvate. Cells were then washed 3 times with PBS and the pellet fraction was extracted with RIPA lysis buffer.

Radioactive S^{35} cysteine/methionine pulse chase assay

HeLa cells were transfected with control or Gα12 siRNA for 72 h in complete DMEM medium. Cells were then washed 3 time with PBS and were cultured in DMEM without L-methionine and L-cysteine for 60 min. Cells were pulsed with 50 μCi S^{35} cysteine/methionine (Perkin Elmer) for 15 min. The cells were washed three times with PBS and chased with complete DMEM medium supplemented with 10%FCS. For BFA treatment, 10 μg/ml BFA was added to the medium for the last 10 min of incubation and kept for the whole experiment. Equal fractions of medium containing secreted proteins were collected at indicated time points, boiled in Laemmli buffer, run on an SDS-PAGE and transferred onto a nitrocellulose membrane. The proteins were visualized by autoradiography using a beta-imager (Biospace Labs). Cells pellets were lysed with RIPA buffer. 20 μL of cell extracts was mixed with scintillation cocktail, and the radioactivity was determined for normalization.

qRT PCR

RNA was extracted from HeLa cells using the RNeasy Mini Kit (QIAGEN) according to manufacturer instructions. The yield and the integrity of RNA were determined by spectrophotometer NanoDrop 2000c (Thermo Scientific) and by TAE agarose gel electrophoresis, respectively. 1 μg of RNA was reverse transcribed using QuantiTect Reverse Transcription Kit (QIAGEN) according to the manufacturer instructions. Analyses were carried out on biological triplicate samples for each experiment and they were processed separately. qRT PCR reactions were performed using the Light Cycler 480® II (Roche), in technical triplicates, on 2 μL of previously diluted cDNA (1:5) template and the LightCycler® 480 SYBR Green I Master Mix (Roche), according to the manufacturer instructions, in the presence of 500nM of specific oligos. The thermal profile consisted of 10 min at 95°C pre-incubation, and 40 cycles at 10sec at 95°C, 10sec at 60°C and 10sec at 72°C. The PCR data were normalized to the average of the reference gene human hypoxanthine-guanine phosphoribosyltransferase 1 (HPRT1). The fold changes in the relative quantifications were calculated according the ΔΔCt method.

XBP-1 splicing assay

To monitor splicing of XBP-1, RNA was extracted from cells subjected to a folding pulse or treated with UPR activators tunicamycin or thapsigargin (RNA easy mini kit, QIAGEN). Approximately 1 μg of RNA from HeLa cells or 100ng of RNA from primary human fibroblasts were reverse transcribed to cDNA (QuantiTect Reverse Transcription kit, QIAGEN). The cDNA was diluted 1:4 in DNase/RNase free water (QIAGEN) and subjected to a PCR with primers that detect both unspliced (u) and spliced (s) XBP-1 (see above) and GAPDH. The PCR products were then run on a 0.8% agarose gel and visualized by UV excitation.

Computational modeling and docking analyses

Predictions of the Sec24A-Gα12 complex were carried out by means of the ZDOCK3.0.2 program (Pierce et al., 2011) . The crystal structure of GDP-bound Gα12 (PDB: 1ZCA) and of Sec24A in complex with Sec23A, Sec22B, and the VSVGct (PDB: 3EGD) were used. The Sec24A portions 346-391, 504-535, 544-741, and 831-1093 as well as the helical domain (i.e., amino acid residues 86-194) of Gα12 were blocked from docking. Docking runs without blocking residues were carried out as well. The VSVGct peptide docked at the B-site of Sec24A was present in all simulations except one, which was carried out to probe the role of the peptide in dictating the Sec24A-Gα12 interface. With the same aim, docking simulations on a Sec24A structure deprived of the ZF domain were run as well. The proteins Sec23A and Sec22B were either present or absent during simulations; when present, their amino acid residues were blocked. A dense rotational sampling was set. The best 2000 solutions from each run were filtered according to the distance (i.e., either 20 Å, 30 Å, or 50 Å distance cutoffs) between the last Cα-atom of VSVGct and the Cα-atom of the amino acid 234 in swII of Gα12. The filtered solutions were subjected to cluster analysis (Root Mean Square Deviation (RMSD) cutoff equal to 3 Å) followed by visual inspection of the cluster centers, according to an approach previously described (Fanelli and Dell'orco, 2008). Consistency was found among the different docking runs. The predicted complex shown herein resulted from docking simulations in the presence of blocked Sec23A and Sec22B, by blocking selected regions of Sec24A (see above) and the helical domain of Gα12, as well as by setting to 30 Å the distance cutoff for filtering docking solutions.

The multimeric complex of COPII-VSVGct-Gα12 was oriented with respect to the surface of a 1,2-dioleoyl-snglycero-3-phosphocholine (DOPC) coarse grained liposome model with a 40nm diameter. On the luminal part of the same surface, the trimeric ectodomain of VSVG in its post-fusion state (PDB: 5I2M) was oriented with the main axis parallel to the z axis and the last amino acid of one protomer in a position that could be reliably connected to the VSVct in the COPII-Gα12 complex. In this framework, the missing amino acid stretch 426-502 connecting the luminal ectodomain with VSVGct was modeled by the "LOOP" subroutine of MODELER (Sali and Blundell, 1993). External α-helical restraints were applied to the amino acid sequence 459-493, according to secondary structure predictions by the Jpred4 server (http://www.compbio.dundee.ac.uk/jpred/). Remarkably, in the predicted model, such a helical region crosses the phospholipid bilayer. Each MODELER run produced 50 models. While completing one VSVG protomer, the other two protomers in the homotrimer were present along with Sec24A-Gα12 predicted complex. Probing different orientations of the VSVG homotrimer with respect to VSVGct led to production of 300 models. One model, characterized by low restraint violations,

absence of bad main-chain dihedrals, and acceptable topology of the transmembrane helix, was used to produce a multimer of three identical units each made of COPII-Gα12-VSVG proteins. It is worth noting that the predicted multimer architecture is one of the many possible. Although the resolution level of the modeled portions especially those in random conformation is expected to be low, the predicted multimer provides a valuable framework to interpret and drive experiments.

Modeling AREX as a local control system

The UPR and the AREX system was cast into a manufacturing scheme based on theoretical principles of automation and manufacturing control. Unfolded cargos are synthesized from amino acids at a nominal synthesis rate of μ_{SP} and they are placed in the unfolded proteins pool. The level of unfolded cargos is denoted with X_{UC}. Unfolded cargos are input to the folding process and are converted into folded proteins at the nominal folding rate of μ_{FP}. The level of folded proteins is denoted with X_{FC}. X_{UC} is specifically sensed by three sensors (PERK, IRE1 and ATF6) and if X_{UC} is below a safe threshold (here called D_{UC}), two control actions namely, synthesis rate control and folding rate control are placed. Indeed, synthesis rate control is activated by PERK and folding rate control is activated by IRE1 and ATF6. Synthesis rate control is performed by a cascade of reactions mediated by PERK dependent eIF2α phosphorylation, synthetically denoted in the figure with α_{UPR}, whose final outcome is to reduce the nominal synthesis rate μ_{SP}. At the same time, a chain of reactions (denoted as β_{UPR}) mediated by IRE1 and ATF6 elicits a transcriptional increase in chaperones, increasing the folding rate. The magnitude of the UPR increases in proportion to the increase in X_{UC}. The export process produces cargo-filled COPII vesicles, at the nominal rate of μ_{EP}. Sec24 senses the level of folded cargos and activates two control actions: the AREX export rate control and AREX synthesis rate control. The AREX synthesis control is performed by the PKR dependent phosphorylation of eIF2α (denoted as α_{AREX}). The final effect of eIF2α phosphorylation is to decrease the synthesis process by means of α_{AREX} and to prevent accumulation of folded cargos in the ER. At the same time Sec24 induces the export rate control action by activating the PKA, ERK and Akt cascades resulting in δ_{AREX}, whose final effect is to enhance the export rate. Black and yellow lines distinguish between the material flow and process flow that are regularly performed in the ER, respectively. The yellow lines denote the flow related to UPR and AREX that are activated only during fluctuations/deviations from the nominal rates.

QUANTIFICATION AND STATISTICAL ANALYSIS

Quantitative fluorescence image analysis

All images for quantitative analysis of cargo arrival to the Golgi after traffic pulses were acquired with an open pinhole (max airy units) and used as originals without any processing or adjustment. Quantitative analysis was performed using the Zen Lite software suite (Carl Zeiss, Germany). In brief, to calculate the amount of cargo in the Golgi after a traffic pulse, the integrated intensity fluorescence (sum) was measured for each cell area and for the Golgi area of that cell and the Golgi/Total ratio was calculated. For experiments with VSVG and PC-I, to correct for background fluorescence, the Golgi/Total ratio at 40°C was subtracted from the Golgi/Total ratio after the traffic pulse. In control cells this value after 16 min was considered as 100% entry of cargo protein into the Golgi and all other treatment conditions were normalized to this value (Golgi/total ratio, %). For experiments with the VSVG-AXA mutant, the Golgi/Total ratio at each time point was normalized to value at 40°C and plotted as fold change over time. The Golgi area was defined in every experiment by using a Golgi resident protein.

For quantitative analysis of total PC-I, all images were acquired with an open pinhole (max airy units) and used as originals without processing or adjustments. Quantitative analysis was performed using Image-J (NIH). In brief, the integrated density of PC-I fluorescence in each cell was divided by the area of the cell. The background fluorescence in each field was corrected for by selecting an equal area outside the cell. The background fluorescence elicited by the PC-I antibodies was corrected for by calculating the staining intensity after treating fibroblast cells with cycloheximide for 2 h at 37°C (to clear the secretory pathway of most of the PC-I) (Forster et al., 2006; Pulvirenti et al., 2008) and subtracting this value from the experimental values. The integrated density/area ratio was then plotted.

Cryo-immuno EM

For surface density calculations, the number of VSVG-GFP nanogold particles associated with a Sec24A positive vesicular tubular cluster (VTC) was counted, and the membrane length was measured using the iTEM software. The density was then expressed as LD (number of gold particles/nanometer).

FRET measurements

cAMP production and PKA activity were measured by the CFP:YFP emission ratio by in live cells. First, cAMP response of the transfected EPAC YFP/CFP FRET pair in HeLa cells placed in glass-bottomed 35-mm dishes (MatTek) was measured using the non-hydrolysable cAMP analog 8-Br-cAMP at 0, 1, 5, 10, 15, 25 and 50 μM to establish a calibration curve.

After the folding and transport pulses, the ROI for the perinuclear area (Golgi) was adjusted and processed using the MetaMorph software using a threshold to select where the VSVG-mcherry was present at the end of the experiment. A peripheral ER signal was selected using equal dimension ROIs on a near area outside the Golgi. CFP:YFP average intensity ratios were calculated for several

ROIs (Golgi or ER) and represented; the average relative ratios were calculated for 10 cells/treatment. The relative cAMP levels were measured after the folding pulse in accordance with the slope of the calibration curve.

Densitometric Analysis

Western blots were exposed to X-Ray films and the exposure times were varied to obtain appropriate signal intensities of protein bands. The films were subsequently scanned and each of the bands were quantitated using the Image-J gel analysis tool.

Statistical Analysis

p values were calculated comparing control and each treated group individually using Student's t test. All statistical parameters are listed in the corresponding figure legends.

Cell

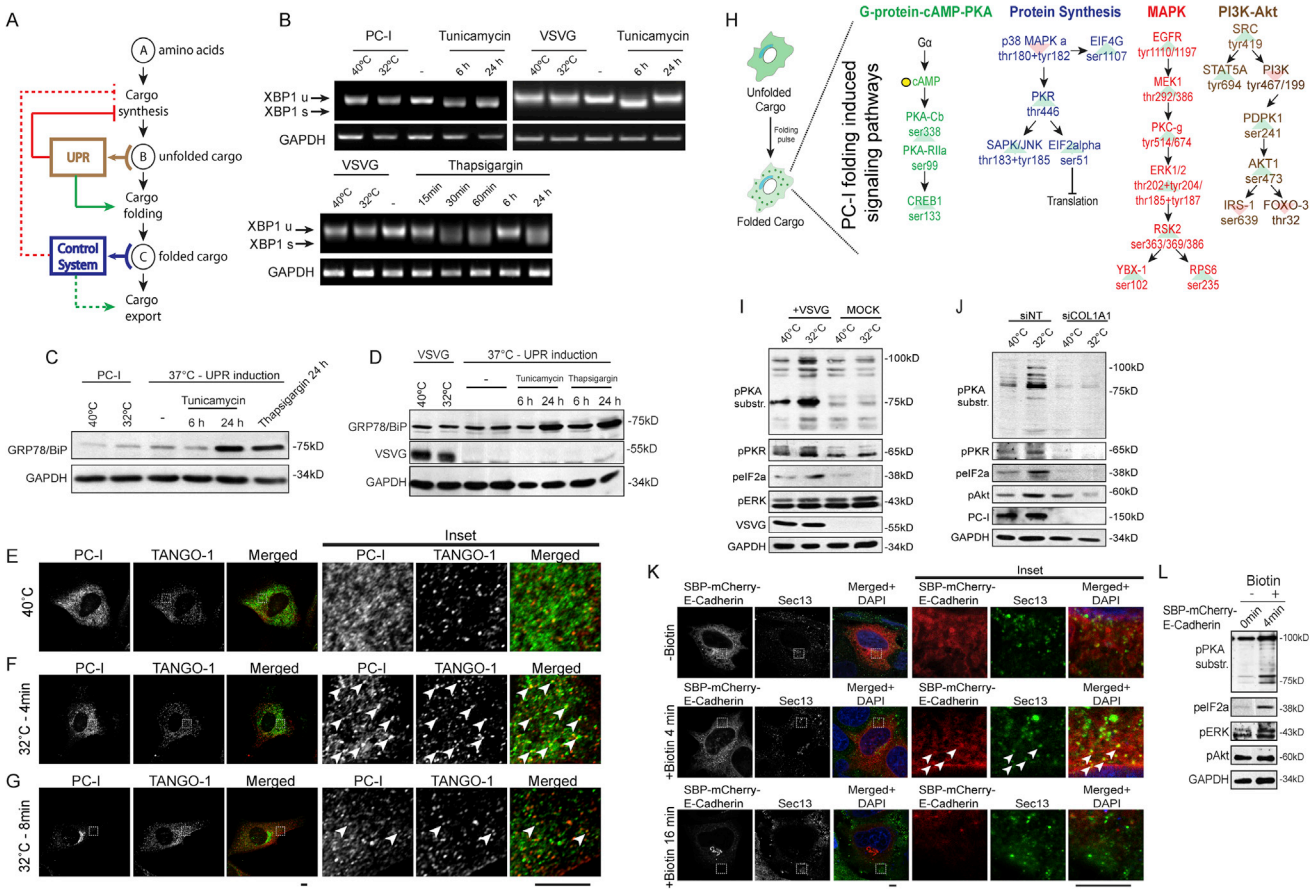

Figure S1. Cargo-Induced Signaling Does Not Trigger the UPR and Is Independent of Temperature Shift or Cycloheximide Treatment, Related to Figures 1 and 2

(A) Schematic representation of the Auto-regulatory or control system hypothesis. The biosynthetic steps leading to folded cargo that is ready for export in the ER are depicted. The inputs/outputs connecting these processes are marked by circles. Control systems are composed of sensors that feed into the controller/effector apparatus (boxes) to regulate the transport process in a positive (green) or negative (red) manner. Our hypothesis is that a control system (blue box) senses the levels of folded cargo in the ER and generates a response to prevent cargo accumulation in a similar manner to the functioning of the UPR that senses unfolded proteins (brown box).

(B) XBP1 splicing analyzed by polymerase chain reaction in response to PC-I or VSVG accumulation and compared to cells at 37°C with or without tunicamycin (2 μg/mL) or thapsigargin (2 μM); XBP1u – unspliced XBP1; XBP1s – spliced XBP1.

(C) Western blotting analysis of BiP/GRP78 in response to PC-I accumulation and compared to cells at 37°C with or without tunicamycin (2 μg/mL) or thapsigargin (2 μM).

(D) Western blotting analysis of BiP/GRP78 in response to VSVG accumulation and compared to cells at 37°C with or without tunicamycin (2 μg/mL) or thapsigargin (2 μM).

(E) IF staining of PC-I and ERES marker TANGO-1 in primary human fibroblasts cultured at 40°C for 3 h without ascorbate (folding block). Cells were treated with cycloheximide for 30 min before folding or transport pulses.

(F) IF staining of PC-I and ERES marker TANGO-1 in primary human fibroblasts shifted to 32°C for 4 min with 100μg/mL ascorbate (folding pulse) after folding block. White arrows depict colocalizing puncta.

(G) IF staining of PC-I and ERES marker TANGO-1 in primary human fibroblasts shifted to 32°C for 16 min with 100μg/mL ascorbate (transport pulse) after folding block. White arrows depict colocalizing puncta.

(H) PC-I folding pulse induced phosphorylation (green arrow) or de-phosphorylation (red arrow) of multiple proteins enriched in signaling pathways and derived from the ranked list. Cell lysates were analyzed by a targeted phosphoproteomic approach based on large microarrays of antibodies against phosphorylated sites in kinases and other regulatory proteins to detect the phosphorylation cascades activated by the challenge, as these might help to unravel the putative mechanisms of the autoregulatory device at the ER. Only the changes in phosphorylation of proteins were analyzed by bioinformatics tools such as KEGG pathways and PhosphositePlus and manually built into signaling pathways. The degree of change in phosphorylation at 32°C was normalized to the baseline value at 40°C and a ranked list was established. Only changes with a Z score > / < 1.00 were considered significant and included induced phosphorylation (green) or de-phosphorylation (red) of multiple proteins enriched in signaling pathways. A subset of proteins depicting the main signaling pathways are represented (see Table S1 for a full list). Connecting arrows depict the canonical signal transduction cascade. Proteins marked in color represent bonafide hits in the assay. Each specific color represents a pathway/network. Proteins marked in black represent putative regulatory proteins (such as kinases/phosphatases) that were included to complete the pathway or network. Second messengers were marked with yellow circles.

(legend continued on next page)

(I) Western blotting analyses of the PKA substrate phosphorylation (between 100kD and 50kD), PKR, eIF2α and ERK1 or ERK2 phosphorylation in HeLa cells expressing VSVG under folding block (40°C) and folding pulse (32°C – 4 min) conditions. Cells not expressing VSVG and subjected to the same folding pulse protocol serve as a negative control.
(J) Western blotting analyses of the PKA substrate phosphorylation (between 100kD and 50kD), PKR, eIF2α and Akt phosphorylation in primary human fibroblasts expressing PC-I under folding block (40°C) and folding pulse (32°C – 4 min) conditions. Fibroblasts depleted for COL1A1 by siRNA and subjected to the same folding pulse protocol serve as a negative control.
(K) IF staining of transfected SBP-mCherry-E-Cadherin and ERES marker Sec13 in HeLa cells cutured at 37°C without biotin (panel 1) and treated with 40μg/mL biotin for 4 min (panel 2) and 16 min (panel 3). White arrows depict colocalizing puncta
(L) Western blotting analyses of the PKA substrate phosphorylation (between 100kD and 50kD), eIF2α, ERK1 or ERK2 and Akt phosphorylation under SBP-mCherry-E-Cadherin ER block (-biotin) and a short biotin pulse (+biotin – 4 min) conditions.
For panels E.) – G.) and K.), scale bars, 10μm.

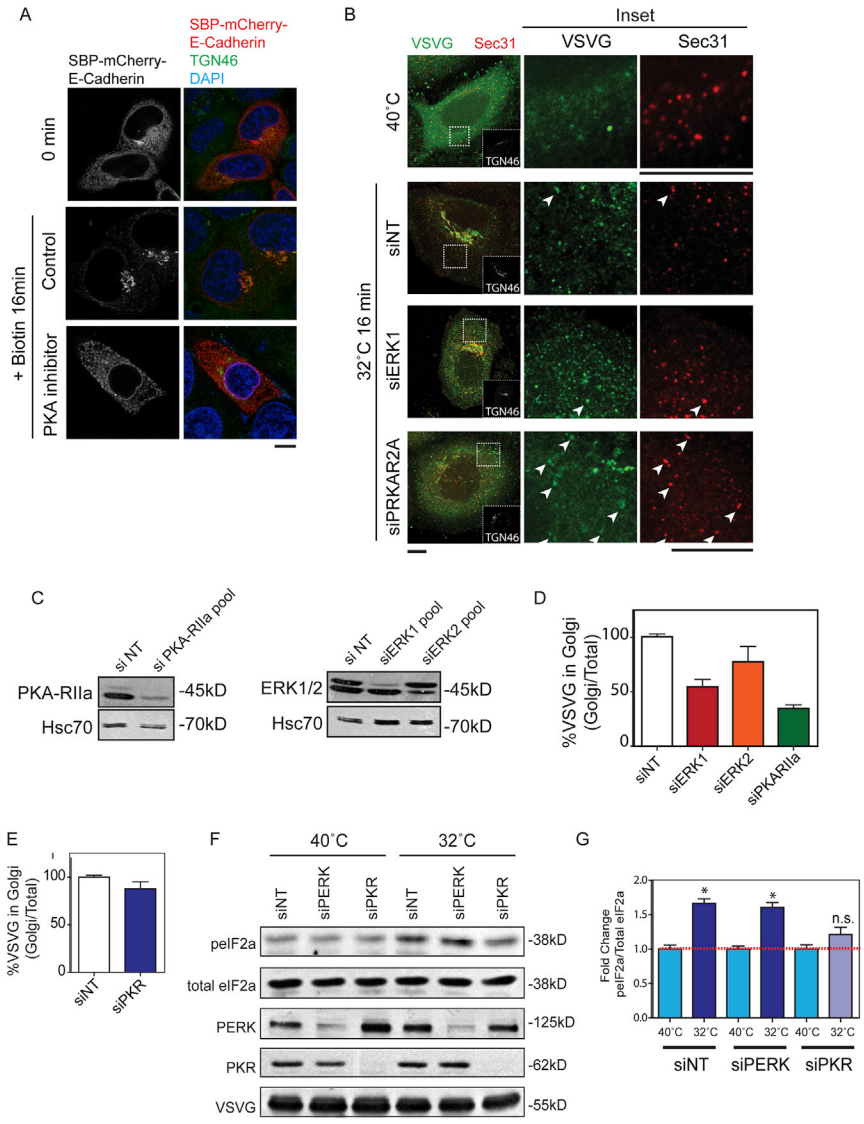

Figure S2. The Cargo-Activated Kinases Regulate ER Export and Protein Synthesis, Related to Figure 3

(A) IF staining of SBP-mCherry-E-Cadherin and Golgi marker TGN46 subjected to a biotin transport pulse (0' no biotin; 16' +biotin) with or without PKA inhibitor (PKI-1422, 100μM). Scale bar, 10μm.

(B) IF staining for VSVG, the ERES marker Sec31 and Golgi marker TGN46 after a cargo transport pulse in cells treated with non-targeting siRNAs, ERK1, and PKA-RIIa siRNAs. White arrows depict cargo and Sec31 colocalizing puncta. Scale bars, 10μm.

(C) Representative western blots corresponding to HeLa cells depleted for PKA-RIIa, ERK1 and ERK2 with siRNAs.

(D) Percentage transport of VSVG from ER to the Golgi in HeLa cells treated with a pool of siRNAs against ERK1, ERK2 or PKA-RIIa (PKAR2A) for 72 h and normalized to non-targeting siRNA control (n = 100 – 150 cells, mean ± standard error of the mean).

(E) Percentage transport of VSVG from ER to the Golgi in HeLa cells treated with a pool of siRNAs against PKR for 72 h and normalized to non-targeting siRNA control (n = 100 cells, mean ± standard error of the mean).

(F) HeLa cells transfected with non-targeting siRNAs, PERK or PKR siRNAs for 72 h, subjected to a VSVG folding pulse and analyzed for eIF2α (S51) phosphorylation by western blotting.

(G) Fold change in eIF2α phosphorylation after VSVG folding pulse normalized to intensity under folding block conditions (n = 4, mean ± standard error of the mean). p values were calculated by Student's t test; **p < 0.01; n.s. not significant.

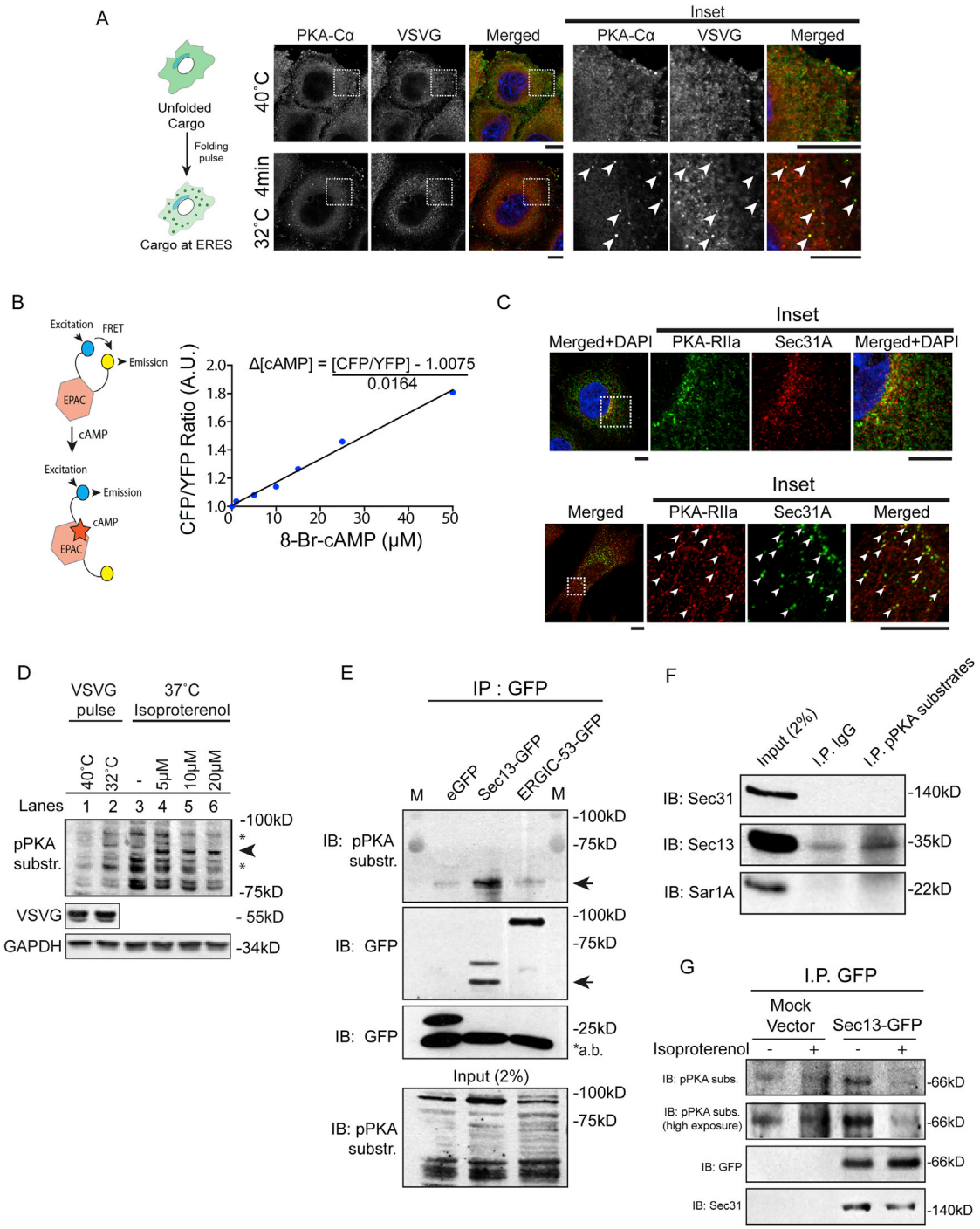

Figure S3. AREX-Dependent PKA Activation at the ERESs Is Segregated from Other PKA-Dependent Pathways, Related to Figure 4

(A) IF localization of PKA-Cα and VSVG under folding block and folding pulse conditions. Scale bars, 10μm. White arrows depict colocalizing pucta.

(B) HeLa cells expressing the EPAC- CFP:YFP FRET pair were incubated with 1, 5, 10, 15, 25 and 50 μM 8-Br-cAMP and the CFP:YFP ratio was calculated to establish a calibration curve. The slope of the curve was in turn used to calculate relative cAMP levels during a cargo folding pulse.

(C) IF staining of PKA-RIIa and ERES marker Sec31 in resting HeLa cells and human fibroblasts. Scale bars, 10μm. PKA-RIIa was mostly diffuse in unperturbed cells, but a few PKA puncta colocalized with the ERES marker Sec31A, a picture intermediate between that seen at 40°C and during a folding pulse (4 min after shift to 32°C).

(D) Western blotting analyses of PKA substrate phosphorylation (between 100kD and 75kD) in HeLa cells after a VSVG folding pulse or stimulation with different concentrations of isoproterenol for 5 min. * - depicts bands induced upon cargo folding; arrow depicts a band induced upon isoproterenol treatment. The phosphorylation levels of some PKA substrates were of an intensity higher than when cargo was unfolded at 40°C; and in some cases almost equivalent to the

(legend continued on next page)

intensity during the folding pulse (compare lanes 1, 2 and 3; * bands), altogether suggesting that basal traffic moderately activates PKA at the ERES . We note here that the pattern in unperturbed cells includes not only AREX-dependent bands but also other bands that are most probably phosphorylated due to stimulation of PKA at other stations of the secretory pathway, such as the Golgi (Cancino et al., 2014).

(E) pEGFP, Sec13-GFP and ERGIC-53-GFP transfected and immunoprecipitated from HeLa cells and probed with the PKA substrate phosphorylation antibody by western blotting.

(F) PKA- phosphorylated substrates immunoprecipitated (IP) from the HeLa lysates using an antibody that enriches all peptides or proteins carrying the consensus (K/R)(K/R)X(Sp/Tp) sequence motif. Western blotting was performed to detect enrichment of COP-II proteins in the IP fractions.

(G) Sec13-GFP immunoprecipitated from HeLa cells stimulated with 20 μM isoproterenol for 5 min and probed with PKA substrate phosphorylation antibody by western blotting. The co-immunoprecipitation with Sec31 served as a positive control.

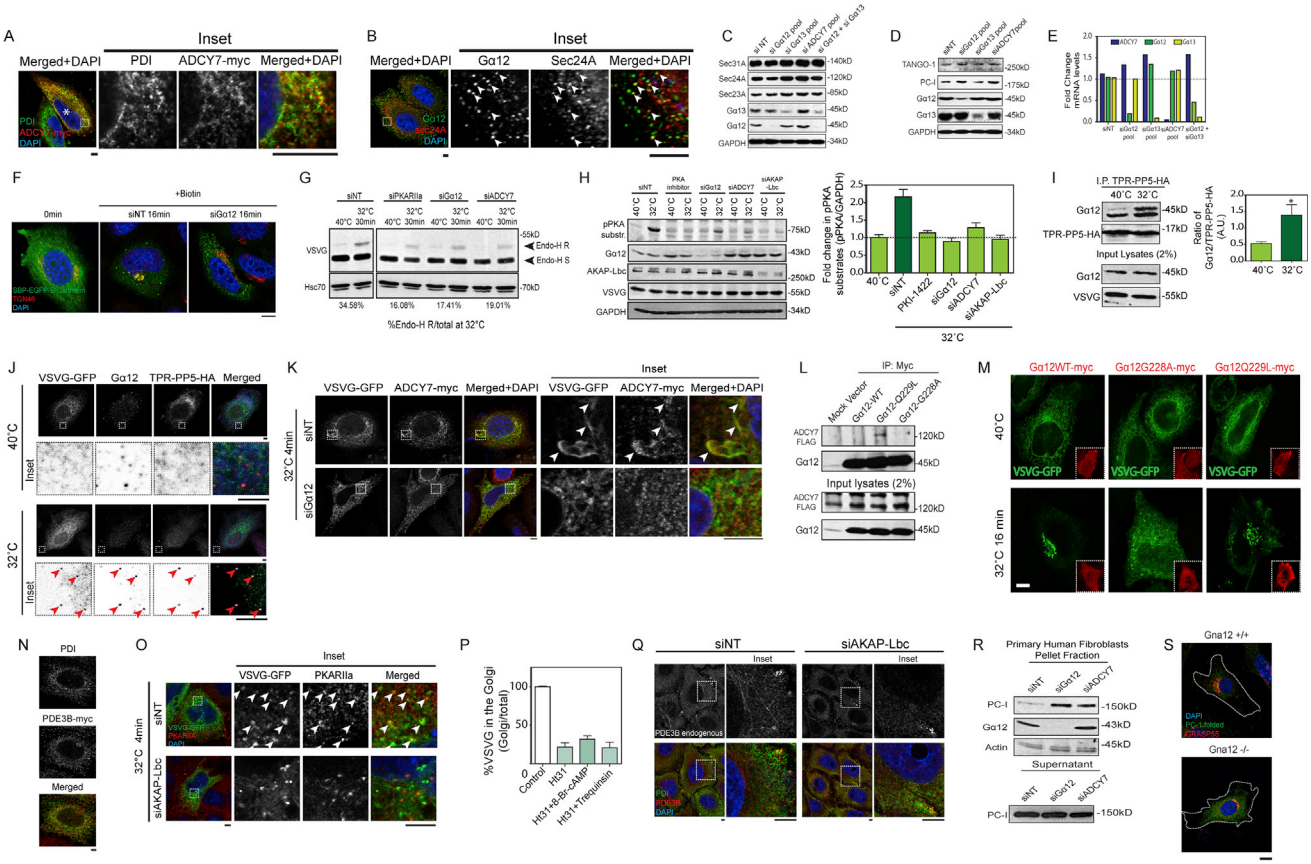

Figure S4. AREX Signaling Components Regulate Cargo-Dependent PKA Activation and Both Pulsed and Steady-State Cargo Export, Related to Figures 5 and 6

(A) IF staining of transfected ADCY7-myc and ER marker Protein disulphide isormerase (PDI) in resting HeLa cells. Scale bar, 5μm.

(B) IF staining of endogenous Gα12 and ERES marker Sec24A in resting HeLa cells. Scale bar, 5μm.

(C) Knockdown efficiencies of a pool of siRNAs (50nM) against Gα12, ADCY7 and Gα13 as compared to non-targeting controls in HeLa cells by western blotting. COP-II proteins were blotted to determine any off target effects on the ER export machinery.

(D) Knockdown efficiencies of a pool of siRNAs (50nM) against Gα12, ADCY7 and Gα13 as compared to non-targeting controls in human fibroblasts by western blotting. TANGO-1 and COP-II proteins were blotted to determine any off target effects on the ER export machinery.

(E) Knockdown efficiencies of a pool of siRNAs (50nM) against Gα12, ADCY7 and Gα13 as compared to non-targeting controls in HeLa cells by qRT-PCR.

(F) IF staining of SBP-EGFP-E-Cadherin and Golgi marker TGN46 in cells after a ER to Golgi transport pulse (16 min + biotin) under non-targeting siRNA or Gα12 siRNA treatments. Scale bar, 10μm.

(G) HeLa cells transfected with non-targeting, PKA-RIIa, Gα12 or ADCY7 siRNAs (50nM) were infected with VSVG virus for 3 h at 40°C and induced to fold and exit the ER at 32°C for 30 min. Cell lysates from each condition were denatured and then treated with the Endo-H enzyme and analyzed by western blotting for VSVG and Hsc70. Arrows indicate Endo-H resistant (Endo-H R or Golgi processed form) or Endo-H sensitive (Endo-H S or ER processed form). The amount of Golgi glycosylated VSVG was calculated by the densitometric ratio between the Endo-H resistant form and the total amount of infected VSVG in each sample and expressed as a percentage.

(H) Fold change in PKA substrate phosphorylation signal intensity after VSVG folding pulse (32°C – 4 min) normalized to intensity under folding block (40°C – 3 h) conditions in cells treated with PKA inhibitor (PKI-1422; 100μM) or non-targeting siRNAs, Gα12, ADCY7 or AKAP-Lbc siRNAs. Histograms represent intensities of PKA-phosphorylated substrate bands corresponding to molecular weight (M.W.) ranges of 100kD – 75kD, 75kD – 50kD and 50kD – 37kD. Data represent the mean ± standard error of the mean for the three (M.W.) ranges on the same gel.

(I) Co-immunoprecipitation and western blotting analyses of endogenous Gα12 and transfected TPR5-PP5-HA under VSVG folding block and folding pulse conditions. TPR-PP5-HA is utilized as bait. Densitometric quantification of Gα12/TPR-PP5 ratio in the immunoprecipitated fractions are plotted (n = 3, mean ± standard error of mean; p values calculated by Student's t test *p < 0.05).

(J) IF localization of VSVG-GFP, Gα12 and transfected TPR-PP5-HA under folding block and folding pulse conditions. Scale bars, 5μm. Red arrows depict colocalizing puncta.

(K) IF localization of transfected VSVG-GFP and ADCY7-myc after a folding pulse (32°C – 4 min) in cells treated with non-targeting siRNAs or Gα12 siRNAs. Scale bar, 5μm.

(L) Co-immunoprecipitation and western blotting analyses of ADCY-FLAG co-transfected with constructs encoding myc-tagged Gα12-WT, GDP-locked Gα12 (Gα12-G228A-myc) or GTP-locked Gα12 (Gα12-Q229L-myc).

(M) IF staining of VSVG-GFP in cells co-transfected with Gα12-WT-myc, Gα12-G228A-myc or Gα12-Q229L-myc (inset) and subjected to an ER to Golgi transport pulse (40°C to 32°C 16 min). Scale bar, 10μm.

(legend continued on next page)

(N) IF staining of transfected PDE3B-myc and ER marker PDI in resting HeLa cells. Scale bar, 5μm.
(O) IF localization of PKA-RIIa and VSVG-GFP after a folding pulse (32°C – 4 min) in cells treated with non-targeting siRNAs or AKAP-Lbc siRNAs. Scale bar, 5μm.
(P) Percentage transport of VSVG from ER to the Golgi in HeLa cells treated with Ht31 peptide (20 μM) alone or in combination with 8-Br-cAMP or trequinsin hydrochloride (PDE3 inhibitor) and normalized to DMSO (vehicle) control. (n = 20 – 35 cells, mean ± standard error of the mean).
(Q) IF localization of endogenous PDE3B and ER marker PDI in resting HeLa cells treated with non-targeting siRNAs or AKAP-Lbc siRNAs. Scale bar, 5μm.
(R) Western blotting of PC-I in the pellet and supernatant fractions of primary human fibroblasts cultured at 37°C treated with non-targeting siRNAs, Gα12, or ADCY7 siRNAs for 72 h. 2 μg/mL ascorbic acid was added in the last 24 h to stimulate the synthesis, folding and secretion of PC-I into the medium (supernatant).
(S) IF staining of folded PC-I (using the monoclonal hCL (I) antibody) and Golgi marker GRASP55 in $Gna12^{+/+}$ and $Gna12^{-/-}$ MEFs cultured at 37°C. Scale bars, 10μm

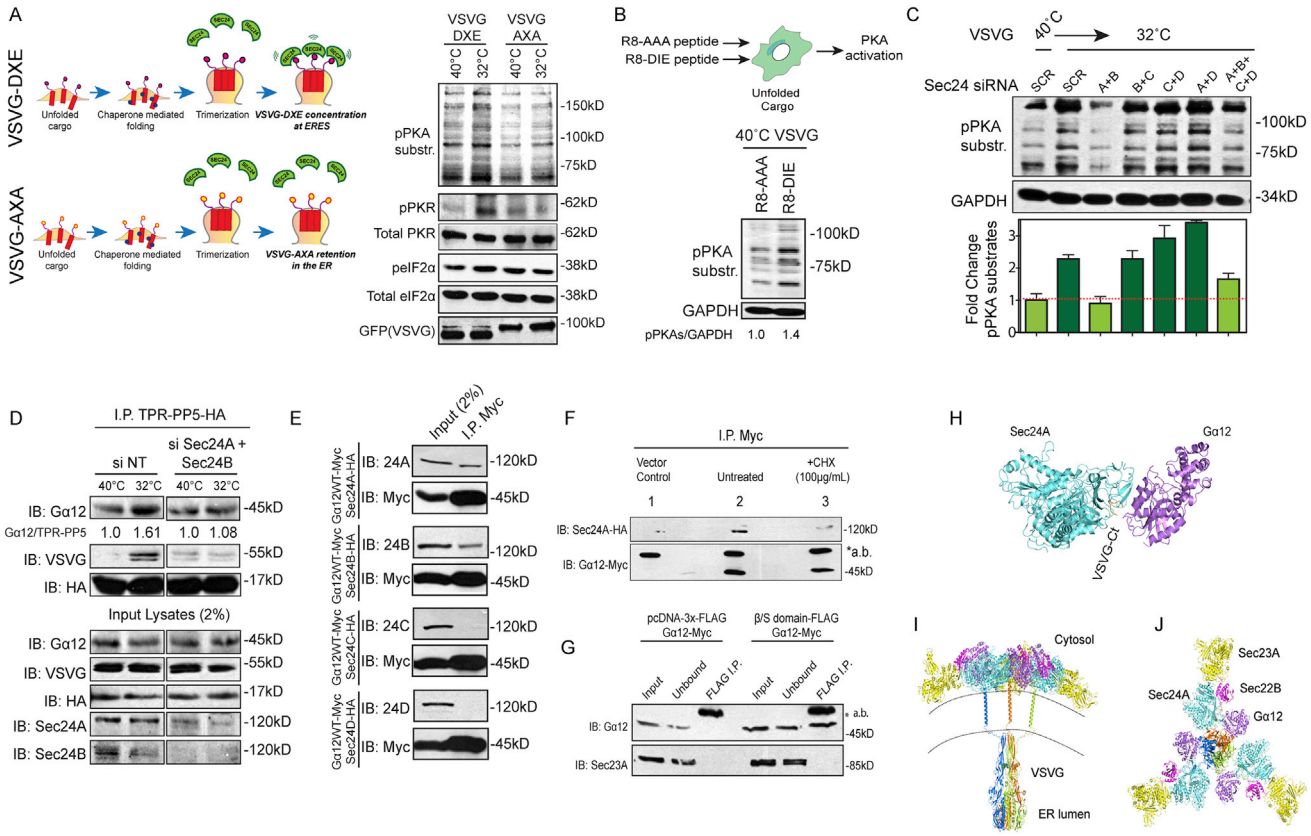

Figure S5. Binding of Cargo Bearing the D-X-E Motif to Sec24A or Sec24B Induces Activation of the AREX Signaling Complex, Related to Figure 7

(A) Western blotting analyses of the PKA substrate phosphorylation pattern, phospho-PKR and phospho-eIF2α in cells subjected to a VSVG-AXA-GFP or VSVG-GFP folding block (40°C 16 h) and folding pulse (32°C – 4 min).

(B) Western blotting analyses of PKA substrate phosphorylation pattern in cells subjected to a VSVG folding block (40°C 3 h) and treated with R8-AAA or R8-DIE peptides (100μM). The fold change of PKA activity normalized to folding block is plotted (n = 2 independent experiments).

(C) Western blotting analyses of PKA substrate phosphorylation pattern in cells subjected to a VSVG folding block and folding pulse under Sec24 scrambled (SCR) siRNA or co-depletion using siRNAs for different Sec24 isoforms (A;B;C;D). The fold change of PKA activity after a folding pulse, normalized to folding block is plotted (between 100kD and 75kD; n = 2).

(D) Co-immunoprecipitation and western blotting analysis of endogenous Gα12, VSVG and TPR-PP5-HA in cells treated with Sec24 scrambled or Sec24A and Sec24B siRNAs and subjected to a VSVG folding block and folding pulse. Normalized densitometric ratio of Gα12/TPR-PP5-HA in the IP fractions are represented below the individual Gα12 bands.

(E) Co-immunoprecipitation of Gα12-myc co-transfected with individual isoforms of HA-tagged Sec24 (A/B/C/D) at 37°C and analyzed by western blotting.

(F) Co-immunoprecipitation of Gα12-myc co-transfected with HA-tagged Sec24A at 37°C without or with treatment with cycloheximide (100μg/mL) for 3 h to clear the secretory pathway of cargo.

(G) The β/S domain of Sec24A (aa 744 – 828) synthesized and cloned into a C-terminal FLAG-tagged construct, co-transfected into HeLa cells with myc-tagged Gα12 and immunoprecipitated with FLAG monoclonal antibody (n = 2).

(H) Cartoon of the predicted complex between Sec24A (aquamarine), Gα12 (violet), and the VSVG C-terminal peptide 502-508 (VSVGct, orange). Exposed residues on the Sec24A ZF and beta sandwich domains make predicted salt bridges with corresponding amino acids on Gα12. The β strand 456-460 from the ZF domain of Sec24A overlaps in part with a part of the AGS protein Girdin/GIV (GIV peptide) in complex with Gαi3, which docks in the swII/α3 cleft of the G protein.

(I and J) The predicted COPII-Gα12-VSVGct complex is compatible with VSVGct being part of a cargo protein characterized by transmembrane and luminal regions. In this respect, computational modeling suggests that the VSVG homotrimer in its post-fusion form (PDB: 5I2M) can interact simultaneously with three oligomers each made of COPII proteins and Gα12. In panels (I.) and (J.) the cartoons of such a multimer made of the three protomers of a VSVG homotrimer (green, orange, and blue), each bound to a multimer of Sec24A (aquamarine), Sec23A (yellow), Sec22B (magenta), and Gα12 (violet) are shown viewed, respectively, in directions perpendicular and parallel to the VSVG N-terminal ectodomain main axis (i.e., in directions parallel and perpendicular to a putative membrane surface, respectively). This model is compatible with 1) the role of the VSVG tail bound to the β sandwich domain in the formation of the complex and with the topology required for the Sec24-Gα12 complex to accommodate the VSVG tail emerging from the ER membrane *in vivo* and 2) the hypothesis that Sec24A acts as a GEF by recognizing regions of Gα12 overlapping with those of a peptide motif on Girdin/GIV, a non-receptor GEF that docks in the swII/α3 cleft of the Gαi3 protein.

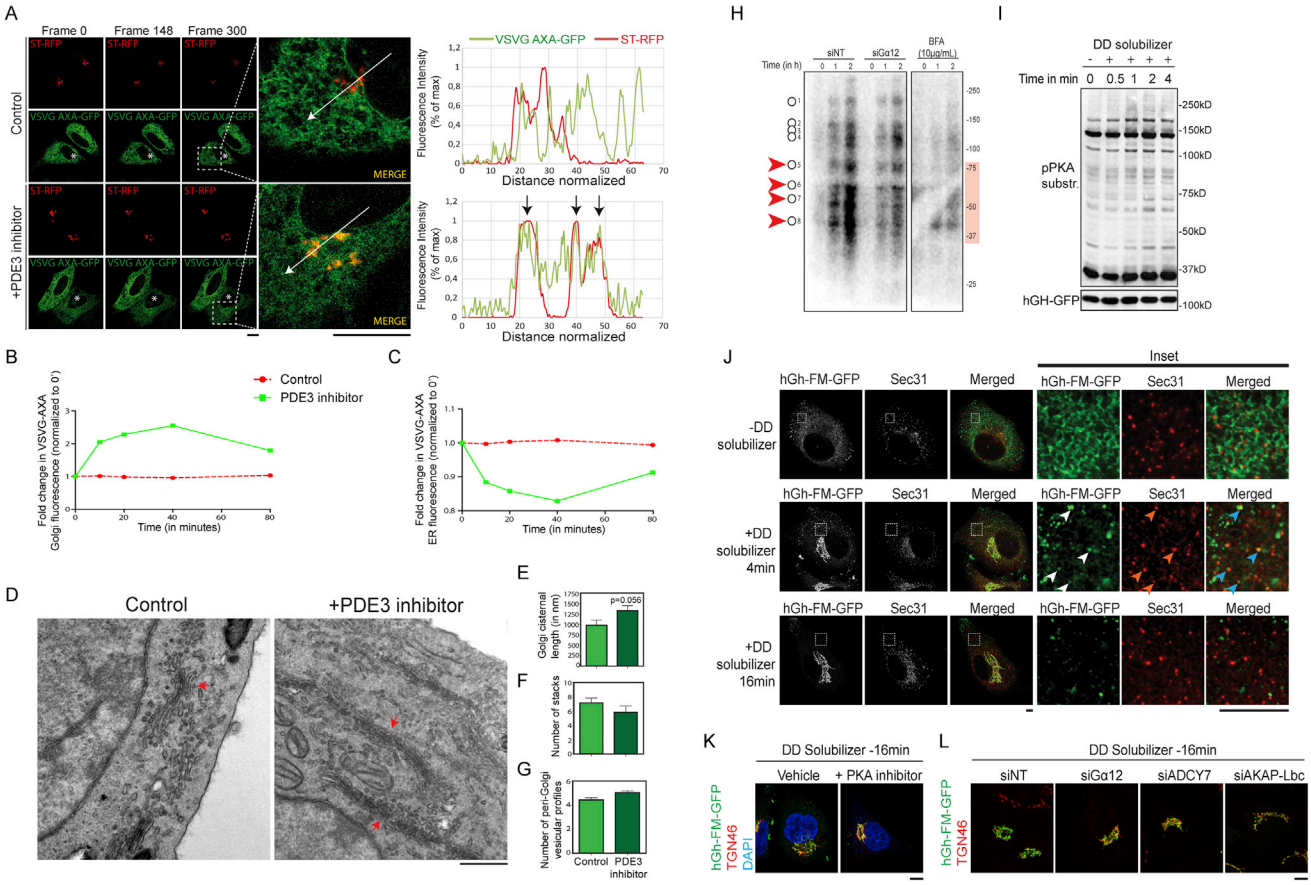

Figure S6. The AREX PKA Pathway Accelerates Bulk Flow Transport and Is Necessary for ER Export of Only a Fraction of Cargoes, Related to Figures 5, 6, and 7

(A) Live cell confocal dual channel imaging of VSVG-AXA-GFP co-transfected with Golgi resident enzyme Sialyl Transferase RFP (ST-RFP) pretreated with DMSO (vehicle) or PDE3 inhibitor (trequinsin hydrochloride 10μM) for 1 h before triggering a cargo transport pulse at 32°C. Representative frames from the movies are shown along with a line scan analysis as a measure of the degree of colocalization in one cell (highlighted with *). Scale bars, 10μm. As expected, after folding, VSVG-AXA-GFP left the ER very slowly and inefficiently without any discernible concentration in the Golgi. Under these conditions, stimulation of PKA at the ER by inhibiting PDE3 markedly accelerated the exit of VSVG-AXA-GFP, indicating that bulk flow out of the ER was enhanced.

(B) Quantification of VSVG-AXA-GFP fluorescence at the perinuclear Golgi area (marked by TGN46) upon treatment with vehicle (DMSO/red) or PDE3 inhibitor (10 μM/green). n = 15 – 20 cells per time point per condition. Average values from each time point are plotted, normalized to time 0 (40°C).

(C) Quantification of VSVG-AXA-GFP fluorescence at the ER upon treatment with vehicle (DMSO/red) or PDE3 inhibitor (10 μM/green). n = 15 – 20 cells per time point per condition. Average values from each time point are plotted, normalized to time 0 (40°C).

(D) HeLa cells were treated with DMSO or PDE3 inhibitor (10 μM) for 1 h and cycloheximide (50 μg/mL) for 30 min at 37°C. Cells were fixed, processed and analyzed by Electron Microscopy (red arrows show Golgi stacks). Scale bars, 500 nm. Representative images are from 15 cells analyzed per condition. The morphometric characterization by EM stereology of the early secretory pathway in cells depleted of cargo (using cycloheximide) and treated with PDE3 inhibitor suggested that the surface area or volume of Golgi stack was significantly increased under these conditions, again consistent with an acceleration of the formation and flow of membrane carriers from the ER to the Golgi.

(E) Quantification of Golgi cisternal length in control and PDE3 inhibitor treatment conditions (n = 25 – 30 Golgi profiles).

(F) Quantification of number of Golgi stacks in control and PDE3 inhibitor treatment conditions (n = 25 – 30 Golgi profiles).

(G) Quantification of number of peri-Golgi vesicular profiles in control and PDE3 inhibitor treatment conditions (n = 25 – 30 Golgi profiles).

(H) Radio-active pulse chase analysis by western blotting of proteins secreted into the medium (20% of the total) of HeLa cells under non-targeting siRNA or Gα12 siRNA treatments. Negative control of the assay is the Brefeldin A (BFA; 10 μg/mL) treated lanes, added 30 min before the pulse. White circles and red arrows represent secreted protein bands. Disabling AREX signaling by depletion of Gα12 resulted in an impaired rate of secretion of a significant fraction of proteins (red arrows), while many other proteins were secreted normally (white circles). This change in the secretome might depend not only on ER export but also on protein synthesis and/or degradation.

(I) Western blotting analyses of PKA substrate phosphorylation pattern in cells subjected to hGH-FM-GFP ER to Golgi transport pulse and lysed at different time points after DD solubilizer (2 μM) addition. Synchronous release of hGH-FMP-GFP did not stimulate PKA substrate phosphorylation at these time points.

(J) IF staining of hGH-FM-GFP and ERES marker Sec31 in cells without DD solubilizer; after 4 min and 16 min of DD solubilizer (2μM) addition. Arrows depict colocalizing puncta. hGH-FM-GFP rapidly concentrated at the ERES and moved to the Golgi.

(legend continued on next page)

(K and L) IF staining of hGH-FM-GFP and Golgi marker TGN46 in cells treated with (K.) vehicle (medium) or PKA inhibitor (PKI-1422; 100μM), and (L.) with non-targeting siRNAs or AREX component siRNAs after 16 min of DD solubilizer (2μM) addition. hGH-FM-GFP export was completely unaffected by the inhibition of PKA or by the depletion of any other AREX signaling component, i.e., under conditions where the export of VSVG, PC-I or E-cadherin was profoundly inhibited. Data from (E), (F), and (G) represent mean ± standard error of mean. p values calculated by Student's t test. Scale bars for (J–L), 10μm.

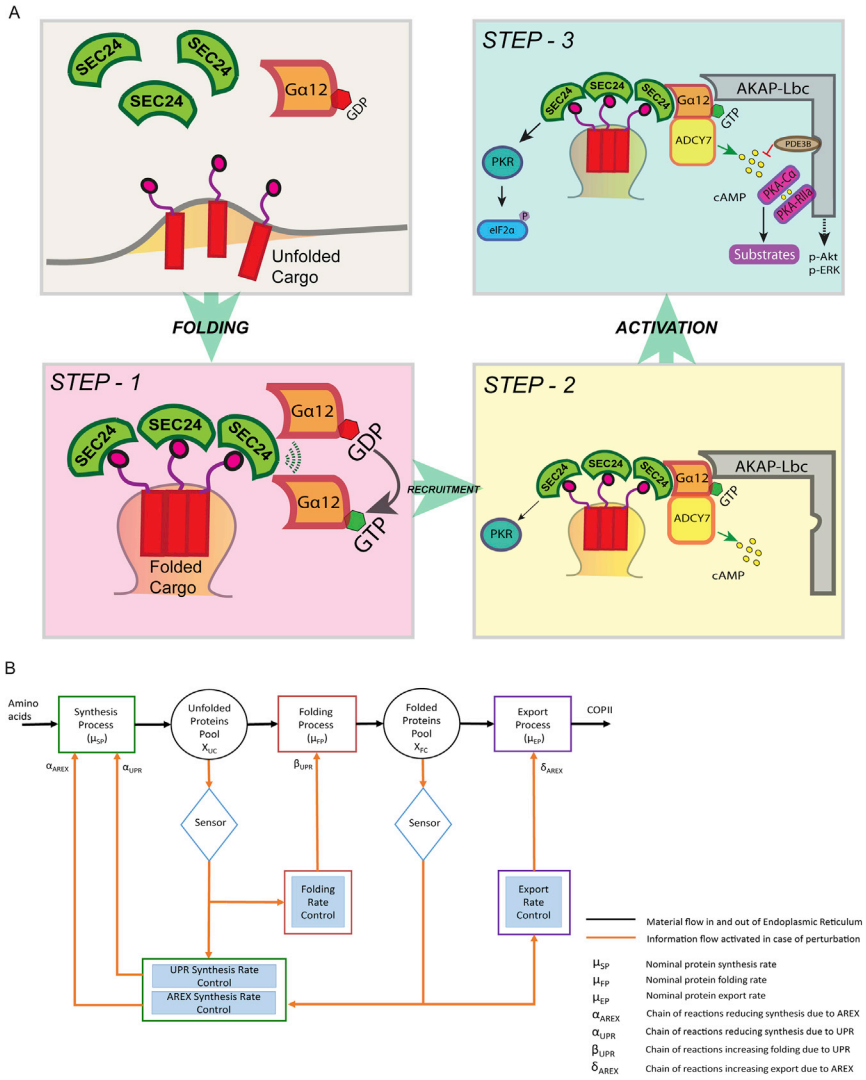

Figure S7. Organization of the AREX-Based Control System, Related to Figures 4, 5, 6, and 7 and STAR Methods

(A) Schematic model of the AREX auto-regulatory signaling cascade assembled by folded VSVG at the ERES. The assembly of AREX is a stepwise process that starts with cargo folding and binding to Sec24. In its unfolded form, VSVG appears unable to bind Sec24 in live cells, whereas folded VSVG interacts with Sec24 robustly, as judged from co-precipitation experiments (Figures 7A and 7B). This effect of folding was unexpected because the isolated VSVG tail peptide is known to bind directly *in vitro* to the Sec24A or Sec24B beta-sandwich domain through its D-X-E motif (Mancias and Goldberg, 2008). It is thus likely that the folding-induced binding of VSVG to Sec24 depends on conditions that occur in live cells during VSVG transport. For instance, unfolded VSVG remains diffuse in the ER, possibly because it is retained by chaperones in the ER matrix (Nehls et al., 2000) (Figure 1C) and is therefore unable to efficiently contact and bind Sec24 *in vivo*. Folded VSVG instead concentrates rapidly at the ERES (where Sec24A localizes) (see Figure 1D), where it can bind Sec24A. Additionally, folded VSVG is likely to interact *in vivo* with the ER cargo adaptor CNIH4, which is required for VSVG transport in mammals (Simpson et al., 2007) as well as for the activation of AREX signaling (our unpublished observations). By analogy with yeast, CNIH4 is needed for forming a CNIH4-Sec24-cargo complex, which is in-turn needed for export (Pagant et al., 2015). Unfolded VSVG most likely does not bind CNIH4, and is thus incapable of stable binding with Sec24. Both of the above mechanisms may explain the folding-dependent binding of VSVG with Sec24 *in vivo*. The cargo-Sec24 complex then binds the G12 family alpha subunit Gα12 (Figures 7A and 7B), resulting in the recruitment of this G-protein to the ERES from an apparently cytosolic localization (Figure 5G). The complex also activates Gα12, i.e., facilitates the GDP-GTP exchange on the G protein, acting as a GEF, as indicated by both *in vivo* and *in vitro* evidence (Figures 7E, 7F, and S5D). Sec24 is structurally different from the canonical GEFs of heterotrimeric G-proteins, namely, the G-protein coupled receptors. However, it appears to belong to another class of G-protein activators called the AGS (Activators of G protein signaling). The AGS proteins are structurally heterogeneous and activate G proteins in different ways (Blumer and Lanier, 2014). An AGS subgroup appears to possess a canonical GEF activity, like Sec24 (de Opakua et al., 2017). A structure of the VSVG-Sec24A-Gα12 interactions is provided by the computational molecular model shown in Figure S5. This model is compatible with 1) the role of the VSVG tail bound to the β sandwich domain in the formation of the complex and with the topology required for the Sec24-Gα12 complex to accommodate the VSVG tail emerging from the ER membrane *in vivo* (Figure S5I), and 2) the hypothesis that Sec24A acts as a GEF by recognizing regions of Gα12 overlapping with those of a peptide motif on Girdin/GIV, a non-receptor GEF that docks in the swII/α3 cleft of the Gαi3 protein (de Opakua et al., 2017). The experimental testing of this model is a task for future work. Once Gα12 is activated, it binds and recruits ADCY7 to the ERES from the ER, where ADCY7 is normally distributed, and stimulates the ADCY7 catalytic activity, enhancing cAMP production locally. Active Gα12 also binds AKAP-Lbc (Diviani et al., 2001) which in turn recruits PKA-RIIa to the ERES

(legend continued on next page)

(Figures 4A and S4O) and anchors PDE3B to the ER (Figure S4Q). The observation that cargo transport from the ER requires the activation of Gα12 (Figures 5A–5E and S4M) and can be rescued by the inhibition of PDE3B in Gα12 depleted cells (Figures 6F and 6G), suggests a role for the local formation of cAMP in the recruitment of PKA. Support for this notion is provided by previous reports that cAMP-activated PKA can auto-phosphorylate the RII subunit (see Figure 2B) inducing an increased binding affinity of this subunit for AKAPs (Manni et al., 2008). Thus, the cargo folding pulse might recruit PKA to AKAP-Lbc at the ERES through an analogous auto-phosphorylation based mechanism, a possibility that remains to be tested. Active PKA then phosphorylates a large number of proteins (Figure 4C) some of which (e.g., Sec13) (Figures 4F, S3E, and S3F) are involved in ER export while others presumably affect other functions. The best characterized AREX arm, the ADCY7-PKA pathway acts at a late stage of the ER export process after the concentration of cargo in budding membrane carriers, by promoting the detachment and/or departure of these carriers toward the Golgi (Figures 3E and 3F and Videos S1 and S2), while the mitogenic signals regulate the early step of cargo concentration at the ERES (Figures 3A and 3B), possibly by promoting the proper assembly of the COPII coat (Farhan et al., 2010). Here, we note that the formation of ER carriers has been previously proposed to be activated by cargo through the stabilization of the COPII coat via the direct binding of cargo to Sec24 during coat formation (Forster et al., 2006; Manzano-Lopez et al., 2015). This stabilization-based mechanism might contribute to the AREX dependent regulation of ER export. Finally, a key effect of AREX is to activate the PKR-eIF2α phosphorylation pathway that attenuates protein synthesis (Figures 2C, S2F, and S2G). Also this step, like the others, is dependent on the interaction between folded cargo and Sec24 (Figure S5A). eIF2α phosphorylation is at the core of a protective cellular mechanism against a number of stress stimuli, termed the integrated stress response (ISR) (Pakos-Zebrucka et al., 2016). Thus, the activation of the ISR by cargo provides an indication of the importance of controlling the folded cargo levels for cell safety. The mechanisms that support PKR activation and eIF2α phosphorylation, and the coordination of this response with the ADCY7-PKA and the mitogenic pathways remain to be elucidated.

(B) The AREX system has the formal features of control systems operating in manufacturing plants. Because AREX senses and regulates folded proteins, while unfolded proteins are sensed and controlled by the UPR, the two control systems AREX and UPR act in sequence and might be connected. We represent both in this scheme. Unfolded cargos are synthesized from amino acids at a nominal synthesis rate of μ_{SP}. The level of unfolded cargos is denoted with X_{UC}. Unfolded cargos are converted into folded proteins at the nominal folding rate of μ_{FP}. The level of folded proteins is denoted with X_{FC}. X_{UC} is sensed by three UPR sensors (PERK, IRE1 and ATF6) and if X_{UC} is below a safe threshold (here called D_{UC}), two control actions namely, synthesis rate control (α_{UPR}) and folding rate control (β_{UPR}) are executed. The task of AREX is to keep the folded cargo levels low. Sec24 senses the level of folded cargos and activates two control actions: the AREX export rate control and AREX synthesis rate control. The export process operates at the nominal rate of μ_{EP}. The AREX synthesis control is performed by the PKR dependent phosphorylation of eIF2α (denoted as α_{AREX}). The final effect of eIF2α phosphorylation is to decrease the synthesis process by means of α_{AREX} and to prevent accumulation of folded cargos in the ER. At the same time Sec24 induces the export rate control action by activating the PKA, ERK and Akt cascades resulting in δ_{AREX}, whose final effect is to enhance the export rate, again to reduce the ER levels of folded cargo. This model can be used to calculate the kinetic behavior of the folded protein levels over time.